Influence of the anchorage shear hysteresis on the seismic response of nonstructural components in RC buildings

Rojas, D.; Quintana Gallo, P.; Pürgstaller, A.; Bianchi, S.; Ciurlanti, J.; Pampanin, S.; Bergmeister, K.

DOI
10.1007/s10518-023-01642-w

Publication date
2023

Document Version
Final published version

Published in
Bulletin of Earthquake Engineering

Bulletin of Earthquake Engineering
https://doi.org/10.1007/s10518-023-01642-w

ORIGINAL ARTICLE

Influence of the anchorage shear hysteresis on the seismic response of nonstructural components in RC buildings

D. Rojas[1] · P. Quintana Gallo[2] · A. Pürgstaller[3] · S. Bianchi[4] · J. Ciurlanti[5] · S. Pampanin[6] · K. Bergmeister[7]

Received: 14 November 2022 / Accepted: 1 February 2023

Abstract
This article presents a numerical study on the influence of the anchorage shear hysteresis on the seismic response of nonstructural components (NSC) connected to multi-storey reinforced concrete (RC) buildings, and of the anchorage itself. To cover a variety of different types of shear hysteresis shapes, this contribution considered the experimental results obtained for five types of post-installed anchors. The results were used for calibrating the hysteresis model of the anchorage connecting an ideal NSC with rigid fixture and a 12-storey RC building host-structure. Using a suit of 40 earthquake records and assuming a single NSC at each storey level anchored by a single fastener, a series of non-linear dynamic analyses of the structure-fastener-nonstructural system was carried out. The results showed significant differences in terms of maximum acceleration and force of the NSC and anchorage, respectively, depending on the type of anchor. These seismic demands were sometimes larger than those required by the reviewed code provisions for rigid NSC, but also for the most restrictive code-case for flexible NSC. The results presented different amounts of scatter, mostly related to the size of the annular gap and of the loading stiffness of the anchorage. It is shown that the maximum force achieved by the anchorage is directly related to the peak relative velocity of the NSC within the gap region. It was concluded that the shape of the shear hysteresis of the anchorage highly influences the response of the NSC and the anchor itself and should not be neglected in practice.

Keywords Nonstructural component · Reinforced concrete · Post-installed anchors · Anchor shear hysteresis · Seismic demand

1 Introduction

Nonstructural components (NSCs) constitute approximately 70% or more of the total investment cost of a building and can be divided into: (1) architectural components; (2) mechanical and electrical equipment; and (3) building contents, based on their functionality (Villaverde (1997); also see FEMA E-74 (2012)) (Fig. 1a). In seismic-prone regions, the

✉ P. Quintana Gallo
patricio.gallo@fsv.cvut.cz

Extended author information available on the last page of the article

Fig. 1 **a** Typical distribution of structural and non-structural parts of buildings (modified after Taghavi and Miranda 2003). Damage to NSCs in Santiago International Airport, Chile, after the 2010 Maule earthquake: **b** damaged ceilings; **c** damaged lift motor (pictures from Cowan et al. 2011)

damage suffered by NSCs during severe earthquakes contributes to most of the economic losses produced by such events (Whittaker and Soong 2003; Taghavi and Miranda 2003). In Chile, for instance, the 2010 Maule earthquake caused severe damage to NSCs, such as those observed at the Santiago International Airport (Figs. 1b, c) which resulted into significant downtime and large repairing costs. Currently, seismic code provisions worldwide, including the Chilean code NCh433 (INN 2012), typically allow damage to NSCs during moderate and large intensity earthquakes. Nevertheless, as part of a damage-control design philosophy (Pampanin 2012), it is desirable to limit the level of damage to both the structural skeleton and the non-structural parts of a building. This growing interest has motivated the study of several researchers aiming at estimating the seismic response of NSCs anchored to multi-storey buildings, with the purpose of improving the design approach as well as developing innovative technical solutions to enhance their performance.

NSCs are commonly fixed to their host concrete structure by means of post-installed anchors (fasteners). It has been highlighted that the response of these NSCs against seismic actions strongly depends on the hysteresis behaviour of the anchor-connection (Pürgstaller 2017; Pürgstaller et al. 2020). Compared to static loads, earthquake-induced actions result in more complex demands on the anchor (Hoehler 2006), including: cyclic loading (tension or shear dominated, or a combination of both), cyclic cracking of concrete, high loading rates, and large crack widths (Eligehausen et al. 2006; Mahrenholtz 2013). Over the past two decades, the primary focus of research on anchor behaviour has been to improve the degree of realism of testing albeit focused at the local (as opposed to system) level. In contrast, there is limited knowledge about how the actual hysteretic behaviour developed in the anchor-connection could affect the expected seismic demands and thus performance of both the NSC and the anchor itself within a building system level (Mahrenholtz 2013; Quintana Gallo et al. 2018).

More recently, numerical research has been undertaken to include the effect on the NSC acceleration response of the shear hysteresis developed in the anchorage, coining the term "Structure-Fastener-Nonstructural Interaction" (SFNI) (Pürgstaller et al. 2020; Fig. 2). The results of such investigation indicated that the seismic factors (i.e., ratio between the design force and the weight of the NSC) prescribed by several code provisions of different countries (see Sect. 2), as well as by those obtained with floor response spectra (see e.g. Adam et al. (2013), Sullivan et al. (2013) and Calvi and Sullivan (2014)), tend to be non-conservative when compared to those obtained through nonlinear dynamic analyses. However, that research: (1) was limited to one type of expansion anchor size M12; and (2) focused on

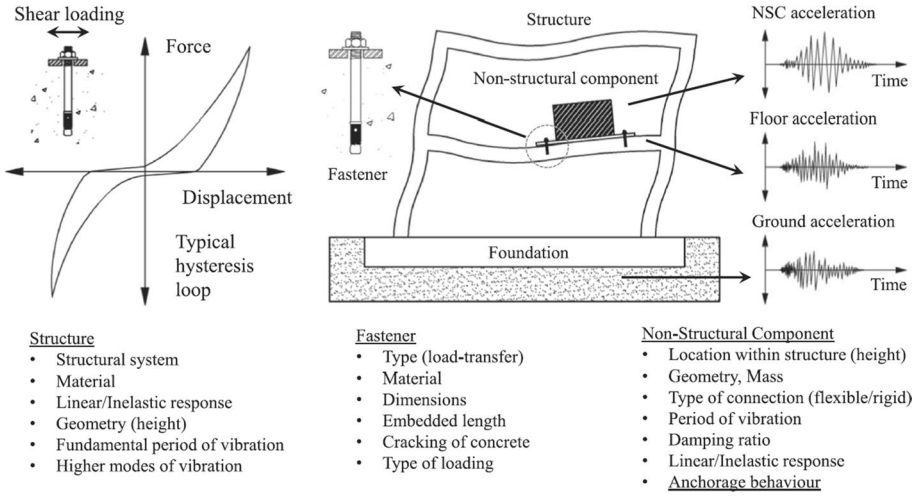

Fig. 2 Structure-Fastener-Nonstructural (SFN) system (after Quintana Gallo et al. 2018; reprinted from Pürgstaller et al. 2020 under Creative Commons CC License)

average values (i.e., did not investigate the scatter of the results); and (3) did not compare the numerical results with the Chilean, New Zealand, and Italian standards provisions.

In this paper, the influence of the hysteretic behaviour of the anchorage response on the seismic demand and performance of a NSC connected to a multi-storey reinforced concrete (RC) building, and of the anchorage performance itself, is investigated. A series of non-linear dynamic analyses (NLDA) is carried out on a 12-storey case study RC building equipped with one NSC at each floor level. The NSC-structure connection includes five alternative anchors: (1) expansion M12 (EM12), (2) EQRod1.1, (3) EQRod1.2, (4) sleeved anchor size M16 (SM16), and (5) sleeved anchor size M10 (SM10). To model the hysteresis of the connection, a recently developed hysteresis model is used (Quintana Gallo et al. 2019). Such model is implemented with the calibration factors suggested in the literature for EM12, and, as part of this research, those calibrated from experimental results for the other anchors. The predicted maximum acceleration and force demands, calculated as the amplification of the peak ground acceleration (PGA) and the maximum floor acceleration subjected to a suit of 40 earthquake records, are compared to those prescribed by different seismic codes, whose requirements are firstly revised.

2 Research significance

Current code provisions use simplified empirical formulae to calculate the design forces for NSCs. A perfectly (fully) rigid connection is typically assumed, neglecting the modelling of the actual hysteresis that occurs in the anchor. This paper extends the work carried out by Pürgstaller et al. (2020), which in fact showed that the inclusion of a realistic hysteresis model for the anchorage within a Structure-Fastener-Nonstructural (SFN) system could result into larger acceleration demands to the NSC, when compared to several design codes: (a) the Chilean standard NCh433Of.96–2012 (INN 2012); (b) the New Zealand standard NZS1170.5:2004 (Standards New Zealand 2004); (c) the Italian code NTC-2018

(Norme Tecniche per le Costruzioni, NTC, Ministero delle Infrastrutture dei Trasporti, MIT 2018); (d) the American code ASCE7 (American Society of Civil Engineers, ASCE 2022); and (e) the European standard Eurocode 8–2004 (European Committee of Standardization, CEN 2004) This extended work: (1) includes four newly calibrated anchors in the analyses, (2) evaluates three additional seismic code provisions for NSC (five in total) and one for the anchorages; and (3) provides a comparison of the results obtained with a set of 40 earthquake ground motions; and (4) provides a new three-dimensional (3D) graphical visualization of the problem, showing the relevance of the velocity of the NSC relative to the host-structure.

3 Seismic provisions for NSCs and anchorages

3.1 Code provisions for NSCs

The Chilean standard NCh433Of.96–2012 (INN 2012) prescriptions for NSCs are based on the tentative requirements of the document ATC3 of 1978 (ATC 1978). According to this Chilean code, the seismic horizontal design force of a NSC (F_{NSC}) is computed with Eq. (1). In addition, for a NSC whose total weight (P_p)—generically named W_{NSC} throughout the paper—is less than 20% of the seismic weight of the floor where it is hosted (P_k), F_{NSC} can be computed with Eq. (2).

$$F_{NCh} = Q_p C_p K_d \tag{1}$$

$$F_{NCh} = \left(\frac{F_k}{P_k}\right) K_p C_p K_d P_p \tag{2}$$

In Eqs. (1) and (2), F_k is the horizontal seismic shear force resisted by the storey level k; P_k is the weight of the storey level k; K_p is a dynamic amplification factor; C_p is a factor tabulated for different types of NSCs (ranges from 0.7 to 2); K_d is the 'performance factor' assigned to the NSC (varies between 0.75 and 1.35). Both C_p and K_d depend on the type of NSC and the importance-category of the structure. The dynamic amplification factor can be taken as $K_p = 2.2$ for all cases, or, alternatively, can be computed by Eq. (3), where $\beta = 1.25(T_p/T^*)$ for $T_p < 0.8\ T^*$; $\beta = 1$ for $0.8\ T^* < T_p < 1.1\ T^*$; and $\beta = 0.91(T_p/T^*)$ for $T_p > 1.1\ T^*$ (T^* is the fundamental period of the structure). Figure 3a presents K_p as a function of T_p/T^*, noting that the peak value is 2.2, the default value required by the code.

$$K_p = 0.5 + \frac{0.5}{\sqrt{\left(1-\beta^2\right)^2 + (0.3\beta)^2}} \tag{3}$$

The standard NCh433 states that, if a static analysis is used, F_k/P_k must be greater than the PGA (or A_0/g as indicated in the NCh433) but does not include this restriction if a modal spectral analysis is used. Even though NCh433 requires the inclusion of the 'anchorage system' in the computation of T_p, it does not specify how to do so. Nevertheless, it requires that if the connection is designed to resist shear actions, the force should be amplified by a factor of A = 2.0.

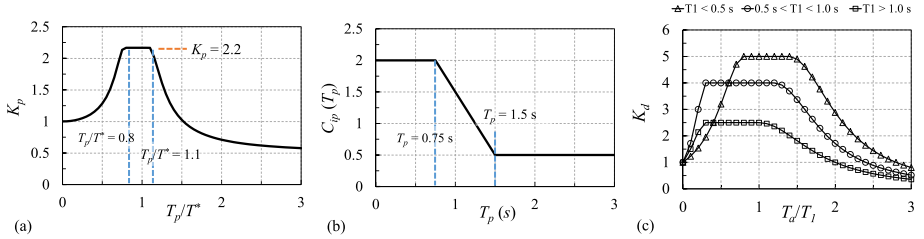

Fig. 3 **a** Dynamic amplification factor, K_p, prescribed by Chilean Standard NCh433; **b** NSC spectral shape coefficient, $C_i(T_p)$, prescribed by NZS1170.5:2004; **c** component amplification factor per NTC-2018

The design force for NSCs prescribed by the New Zealand standard NZS1170.5 (Standards New Zealand 2004), F_{NZS}, is calculated using Eq. (4). In this equation, T_p is the period of the NSC; $C_p(T_p)$ is the horizontal design coefficient of the NSC, given by Eq. (5); C_{ph} is the horizontal response factor for the NSC, which depends on the ductility of the NSC (varies between 1 and 0.45; it is equal to 1 unless yielding of the NSC fixture is expected); and R_p is the NSC risk factor (varies from 0.9 to 2). In Eq. (5), in turn, $C(0)$ is the risk coefficient for a period $T=0$; C_{Hi} is the floor height coefficient of the floor level i, ranging from 1 (at the base) to 3 (at the roof level); $C_i(T_p)$ is the spectral shape coefficient of the NSC (presented in Fig. 3b); and $C(0)$ is given by Eq. (6).

$$F_{NZS} = C_p(T_p)C_{ph}R_pW_p \leq 3.6W_p \tag{4}$$

$$C_p(T_p) = C(0)C_{Hi}C_{ip}(T_p) \tag{5}$$

$$C(0) = C_h(0) \cdot Z \cdot R \cdot N(T, D) \tag{6}$$

In Eq. (6), T is the fundamental period of the structure; $C_h(0)$ is the spectral shape factor for $T=0$, which, for NSCs, is $C_h(0)=1.0$; Z is the hazard factor, determined according to the geographical location of the structure within New Zealand; R is the return period factor (ranges between 0.2 and 1.8; it is equal to 1.0 for the ULS spectrum), limited such that $Z \times R < 0.7$; and $N(T, D)$ is the near-fault factor associated with the existence of nearby geologic faults within a range of 20 km from the site where a structure is located. The parameter C_{Hi} is equal to $(1+h_i/6)$ for $h_i < 12$ m, to $(1+10h_i/h_n)$ for $h_i < 0.2h_n$, and to 3.0 for $h_i \geq 0.2h_n$. The standard NZS1170.5:2004 does not prescribe any lower limit for the coefficient $C_{NZS}=F_{NSC}/W_{NSC}$. This means that the resulting seismic coefficient can eventually be smaller than the PGA, as in the case of flexible NSC with $T_p > 1.5$ s, where $C_i(T_p)=0.5$, as shown in Fig. 3b.

In the Italian code NTC-2018 (MIT 2018), design action for NSC, F_{NTC}, is given by Eq. (7), where S_a is the maximum acceleration, in units of g, of the NSC for a given limit state, W_a is the seismic weight of the NZC, and q_a is the behaviour factor assigned to the NSC (equal to 1.0 or 2.0 depending on the type of NSC).

$$F_{NTC} = \frac{S_aW_a}{q_a} \tag{7}$$

To compute F_{NTC} (Eq. (7)), the spectral acceleration S_a can be calculated with the simplified expression of Eq. (8), applicable to frame buildings. For the scope of this research, this

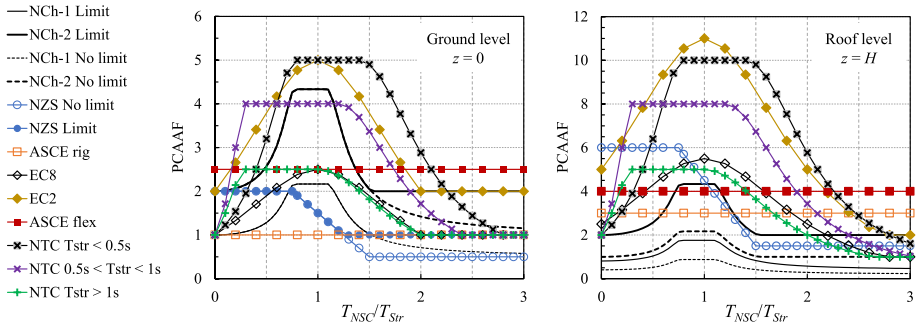

Fig. 4 Comparison of PCAAF for ground and roof levels. *Note* for NZS, $T_{Str}=1$ to enable comparisons with the prescriptions of the other codes

expression is selected, thus used in the case-study example, due to its simplicity when compared to the more general formulation which accounts for different mode of vibrations of the building. In Eq. (8), α is the ratio between the maximum ground acceleration (a_g) for soil type A and the gravity acceleration g; S is a coefficient accounting for both the soil type and the topographic conditions of the site; z is the height of the NSC above the ground, H is the total height of the building, and K_d is given by Eq. (9). In this last equation, T_a is the fundamental period of vibration of the NSC; T_1 is the fundamental (elastic) period of vibration of the structure, and a, b, and a_p are parameters which depend on T_1. Figure 4c presents a graphic with the numerical values of the expressions for K_d depending on these parameters.

$$S_a\left(T_a\right) = \alpha S\left(1 + \frac{z}{H}\right)K_d \geq \alpha S \tag{8}$$

$$K_d\left(T_a/T_1\right) = \begin{cases} \left[\dfrac{a_p}{1+\left(a_p-1\right)\left(1-\frac{T_a}{aT_1}\right)^2}\right] & \text{for} \quad T_a/T_1 < a \\ a_p & \text{for} \quad a \leq T_a/T_1 < b \\ \left[\dfrac{a_p}{1+\left(a_p-1\right)\left(1-\frac{T_a}{bT_1}\right)^2}\right] & \text{for} \quad T_a/T_1 \geq b \end{cases} \tag{9}$$

According to the code ASCE7 (ASCE 2022), the design forces for NSC are determined with Eq. (10), where S_{DS} is the spectral acceleration at ground level; α_p is the amplification factor (1.0 and 2.5 for rigid and flexible NSC, respectively); I_p is the NSC importance factor (1.0 for normal components; 1.5 for components required for life-critical, essential operations or containing hazardous materials); W_{NSC} is the weight of the NSC; and R_p is the component response modification factor (ranges between 1 and 12, and is related to the NSC deformation capability).

$$0.3S_{DS}I_pW_{NSC} \leq F_{ASCE} = \frac{0.4S_{DS}a_pW_{NSC}}{\left(R_p/I_p\right)}\left(1 + \frac{2z}{H}\right) \leq 1.6S_{DS}I_pW_{NSC} \tag{10}$$

The design force prescribed by Eurocode 8–2010 (CEN 2004) for the design of NSC not containing hazardous materials, is Eq. (11).

$$F_{EC8} = \frac{S_a W_a \gamma_a}{q_a} \tag{11}$$

In Eq. (11), S_a is the pseudo-acceleration for the *NSC*, in units of g, γ_a is the importance factor of the NSC (1.5 if the NSC must remain operational after an earthquake, otherwise equal to 1.0); q_a is the behavior factor of the element (1.0 or 2.0); and W_a is the weight of the NSC. The parameter S_a is computed with Eq. (12), where α is the design ground acceleration for soil type A, (a_g) divided by g; S is a factor which depends on the soil type; T_a is the period of the NSC; T_1 is the fundamental (elastic) period of the host structure; z is the height of the NSC above the ground level; and H is the total height of the host structure.

$$\alpha S < S_a = \alpha S \left(\frac{3\left(1 + \frac{z}{H}\right)}{1 + \left(1 - \frac{T_a}{T_1}\right)^2} - 0.5 \right) \tag{12}$$

3.2 Code provisions for anchorages

The Eurocode 2 part 4 (CEN 2018), which superseded the CEN/TS 2009 recommendations, provides requirements for the specific design of anchorages. It uses a similar approach of Eurocode 8–2004 (CEN 2004), with design seismic coefficient, S_a, given by Eq. (13). The amplification factor, A_a, however, can be either calculated with Eq. (14) [which combined with Eq. (13) yields Eq. (12)] or can be, alternatively, obtained from Table C.2 of the code. This table prescribes values of A_a equal to 1.5 or 3, depending on the type of NSC.

$$\alpha S \le S_a = \alpha S \left[\left(1 + \frac{z}{H}\right) A_a - 0.5 \right] \tag{13}$$

$$A_a = \frac{3}{1 + \left(1 - T_a / T_1\right)^2} \tag{14}$$

In addition, Eurocode 2–4 requires the strength of anchors resisting in shear and having an annular gap to be divided by the parameter α_{gap}, which accounts for extra dynamic effects (hammering or impact between fixture and rod, see Quintana Gallo et al. (2018, 2019), Pürgstaller et al. (2020), and Ciurlanti et al. (2022)). Including this factor into the design force leads to Eq. (15).

$$F_{EC2} = \frac{S_a W_a \gamma_a}{\alpha_{gap} q_a} \tag{15}$$

In the case of anchors resisting shear actions and having an annular gap, $\alpha_{gap} = 0.5$, as specified for construction tolerances, which means an amplification of 2.0 of the design forces. Following Pürgstaller et al. (2020) and Ciurlanti et al. (2022), it was noted that this factor should also be included in the calculations of the forces affecting the NSC, as in Eq. (15).

Table 1 Design coefficient for NSCs prescribed by the surveyed design codes

Code (Abbreviation)	PGA	PCAAF		Importance/ risk (I_{NSC})	Performance/ behaviour (S_{NSC})	Weight(W_{NSC})
		Height amplification factor HAF = PFA/PGA	Component amplification factor a_p = PCA/PFA			
NCh433-2012 (NCh)	A_0	$(F_k/P_k)/A_0$	$\alpha_s K_p$	C_p	K_d	P_p
NZS1170.5:2004 (NZS)	$C(0) = Z{\cdot}R{\cdot}N$	$C_{Hi}/C(0)$	$C_{ip}(T_p)$	R_p	C_{ph}	W_p
NTC-2018 (NTC)	αS	$(1 + z/H)$	K_d	-	q_a	W_a
ASCE7-2016 (ASCE)	$0.4S_{DS}$	$(1 + 2z/H)$	a_p	I_p	R_p	W_{NSC}
Eurocode 8 2004 (EC8)	α	S_d/α	Included in HAF	γ_a	q_a	W_a
Eurocode 2–4 2018 (EC2)	α	$S_d/(\alpha\ \alpha_{gap})$	Included in HAF	γ_a	q_a	W_a

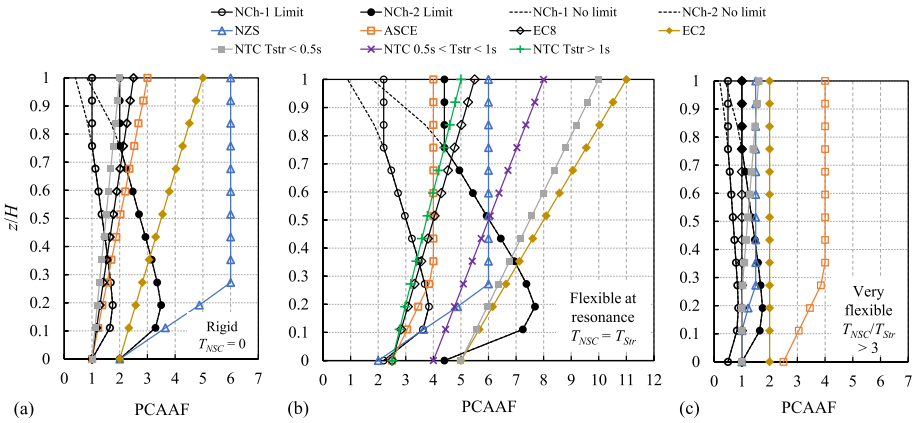

Fig. 5 Comparison of PCAAF of different codes for NSCs: **a** with rigid fixture (T_{NSC}=0) **b** with flexible fixture, at resonance (T_{NSC}=T_{Str}); **c** with very flexible fixture (T_{NSC}/T_{Str} > 3)

3.3 Comparison of code requirements

Table 1 summarizes the design coefficients involved in the calculation of F_{NSC} according to each of the codes reviewed. These coefficients are grouped into four categories: (a) the peak ground acceleration (PGA); (b) the peak component acceleration amplification factor (PCAAF); (c) the importance or risk factor (I_{NSC}); (d) the performance or behaviour factor (S_{NSC}); and (e) the seismic weight of the NSC (W_{NSC}). Figure 4 compares the values of PCAAF prescribed by the different codes as a function of T_{NSC}/T_{Str}, for the ground and roof levels (T_{NSC} and T_{Str} are the NSC and fundamental period of the host structure, respectively). The plots of the NCh433 and NZS1170.5 formulations include the 'as-prescribed' case (with no limitation for PCAAF), and an alternative case, which includes a minimum PCAAF of 1.0 (denoted by 'No Limit' and 'Limit', respectively). Figure 5 presents the

distribution of PCAAF over the height for: (a) NSC with rigid fixture ($T_{NSC}/T_{Str}=0$); (b) NSC with flexible fixture at resonance ($T_{NSC}/T_{Str}=1$); and (c) NSC with very flexible connections ($T_{NSC}/T_{Str}>3$).

Figure 4 depicts how some of the codes prescribe PCAAF as one of the following: a smooth function of T_{NSC}/T_{Str} with a peak value at $T_{NSC}=T_{Str}$ (codes EC8 and EC2); a piecewise function of T_{NSC}/T_{Str} with maximum values in the form of a horizontal plateau located close to the resonance case ($T_{NSC}=T_{Str}$) (codes NCh and NTC); a piecewise-linear function which depends on T_{NSC} only (i.e. T_{Str} is not considered and set to 1.0 for comparison), with an initial plateau (code NZS); and as a constant value, i.e., independent of T_{NSC}/T_{Str}, larger for flexible than for rigid NSCs (code ASCE). The most conservative code prescriptions at the ground and roof levels are those of NTC and EC2, respectively. On the flip side, and if the limitation PCAAF$\geq$1.0 is considered, the less conservative provisions at ground level are those of ASCE for rigid NSC (referred to as ASCE_{rig}). If there is not such a limit, in turn, the requirements of NZS and NCh fall below $\text{ASCE}_{\text{flex}}$ for $T_{NSC}/T_{Str}>1.25$ and >1.5, respectively. For the roof level, NCh requires the less conservative values of PCAAF for the whole period rage examined, even if the restriction PCAAF$\geq$1.0 is included. An exception is the case NCh-2, which included the magnification factor A=2.0, applicable to anchors resisting shear actions. It is worth mentioning that the only difference between PCAAF prescribed by EC8 and EC2 is the factor $\alpha_{gap}=0.5$, which divides the expression of EC8 to become that of EC2.

Figure 5 shows how most of the design codes surveyed prescribe values of PCAAF which linearly increase for increasing values of the location height (z) of the NSC. The exceptions are NZS, which provides a linearly increasing value of PCAAF from $z=0$ to $z=0.2H$ but a constant value of PCAAF=6.0 for $z\geq 0.2H$; NCh, which provides decreasing values of PCAAF from a given z, depending on the results of the seismic analysis of the structure; and ASCE, which establishes linearly increasing values of PCAAF, but limited to a maximum of PCAAF=4.0. The counterintuitive reduction of PCAAF established by NCh is a result of the direct association of the maximum floor acceleration to the maximum shear force demand required at a given storey, which is not a true relationship. The code that prescribes the most restrictive values depends on the flexibility conditions of the NSC. For rigid NSC and the whole period range examined, NZS is the most conservative code, mostly because the factor a_p for rigid NSC is very large (Fig. 3b). For the resonance condition, EC2 provides the most restrictive values of PCAAF, whereas for NSC having very flexible fixing conditions ($T_{NSC}/T_{Str}>3$), ASCE represents the most conservative case.

4 Case study description and numerical modelling

The case study building is a prototype 12-storey RC building, previously studied by Quintana Gallo (2008), designed according to the Chilean seismic standard NCh433Of.96 (INN 1996) and the design code ACI318-05 (ACI Committee 318, 2005). The building also complies with the current Chilean normative and the requirements of the New Zealand standards NZS1170.5 (Standards New Zealand 2004) and NZS3101 (Standards New Zealand 2006), for the same hazard and soil conditions (PGA=0.4 g). The prototype 12-storey RC building is 45.15 m high (first level 5 m, all others 3.65 m) and has a rectangular plan layout extending 55.3 m (7 bays at 7.9 m) and 20.1 m (3 bays at 6.7 m) in the longitudinal (long) and transverse (short) directions, respectively (Fig. 6). The seismic and gravity load resisting system consists of four cantilever T-shaped walls (named TW) and frames

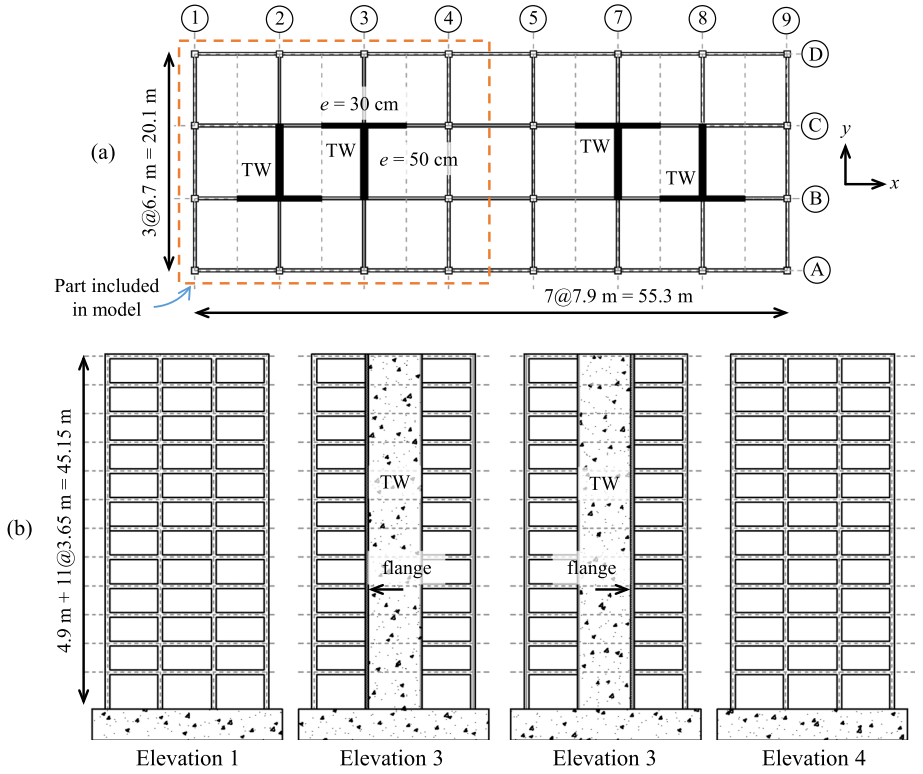

Fig. 6 Prototype structure description: **a** typical plan; **b** elevations included in planar model (Quintana Gallo 2008; Quintana Gallo et al. 2020)

located in the perimeter and the central part of the structure. The walls have 500 mm and 300 mm thick webs and flanges, respectively. The columns had a square cross-section of 550×550 mm (except for the first storey central columns with 650×650 mm), whereas the beams had a rectangular cross-section of 600×250 mm. The floor system consisted of 200 mm slabs. The total seismic weight of the structure is $W_s = 150{,}600$ kN. It was assumed that the concrete had a characteristic compressive strength of $f_c' = 30$ MPa, and the reinforcing steel had yielding and ultimate stresses of $f_y = 420$ MPa and $f_u = 630$ MPa, respectively. Further details on the design features of the host-structure can be found in Quintana Gallo (2008) and Quintana Gallo et al. (2020).

The structure was analysed in the short direction, and further idealized, making use of symmetry, as presented in Fig. 7b. In the numerical model constructed in the computer program Ruaumoko2D (Carr 2017), walls, columns, and beams were modelled with lumped-inelasticity frame elements with plastic hinges in both ends. The moment–curvature hysteresis relationship of the walls was modelled with a tri-linear SINA model, whereas those of the columns and the beams were modelled with a Modified Takeda rule (Saiidi and Sozen 1979). The lateral displacement of the system was constrained at each storey level, simulating the rigid diaphragm action of the floor slabs. The fundamental natural period of the structure in the direction of analysis was computed as $T_{Str} = T_1 = 1.48$ s. The period of the second mode, in turn, was $T_2 = 0.29$ s. The building model was equipped with NSCs

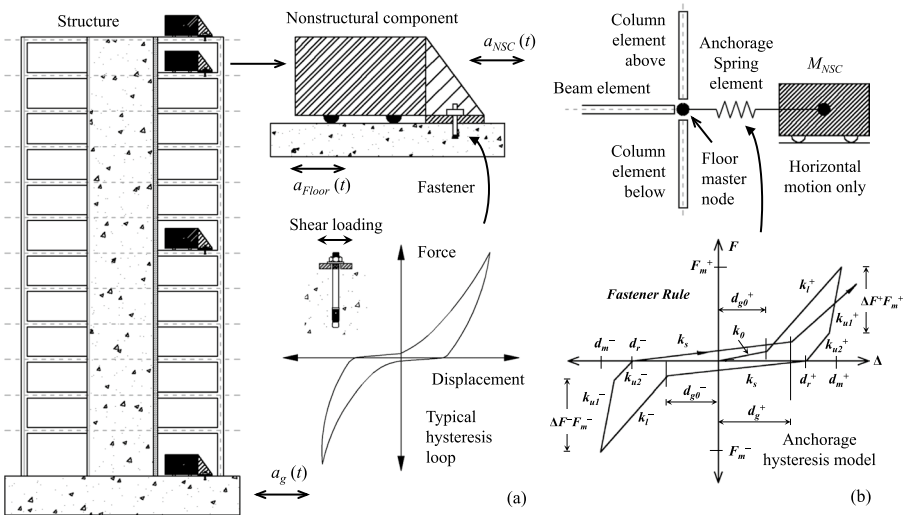

Fig. 7 **a** Idealized structure-fastener-nonstructural (SFN) system definition (Pürgstaller et al. 2020), **b** including the hysteresis model for the anchorage (Fastener Rule, Quintana Gallo et al. 2019)

anchored to each storey level via a single post-installed anchor, conceptually anchored into the slabs such that they resist only shear actions. To simulate the structure-fastener-nonstructural (SFN) system, at each diaphragm level, an extra node was included on the right-hand side of the outermost column, as shown in Fig. 7b. The horizontal inertial mass of the NSC, M_{NSC}, was assigned to this extra node, which in turn was connected to the structure via a spring-type element implemented with the Fastener Rule (FR) hysteresis model (Quintana Gallo et al. 2019). The degrees of freedom of the node were restricted so that there is only displacement in the direction parallel to the axial direction of the spring (horizontal global axis).

5 Properties of the anchorage and NSC

5.1 Anchorage system

The anchors included in this study are: (1) a bolted torque-controlled expansion anchor size M12 (12 mm nominal diameter), herein referred to as EM12; (2) EM12 with a supplemental damper, referred to as EQ-Rod1.1; (3) EM12 with a supplemental damper and plastic cone, referred to as EQ-Rod1.2; (4) a sleeved anchor size M10 (10 mm nominal diameter), referred to as SM10; and (5) a sleeved anchor size M16 (16 mm nominal diameter), referred to as SM16. Figure 8 presents details of the selected anchors. In particular, the features of the EQ-Rod anchors are detailed in Fig. 10b–e. These EQ-Rod anchors include a supplemental device aimed at upgrading the response of the anchorage and of the NSC. Further details are beyond the scope of this paper and are provided in Quintana Gallo et al. (2018). Table 2 presents the effective height of the selected anchors, and their static ($V_{n,stat}$) and seismic ($V_{n,seis}$) nominal shear strengths.

The hysteresis model for the anchorage (Fastener Rule, FR) was calibrated with the experimental data obtained through quasi-static tests of the anchors subjected to shear

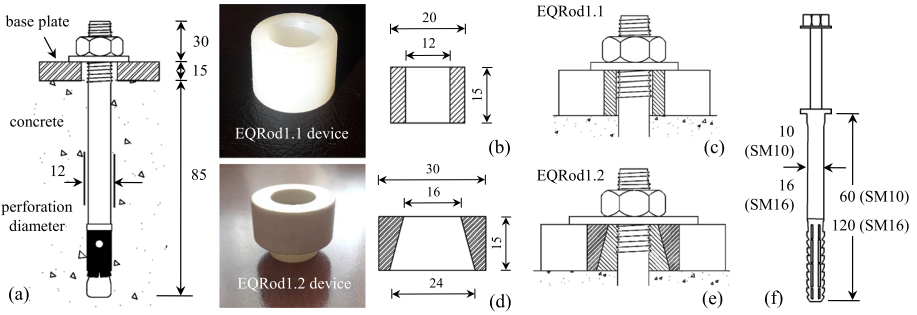

Fig. 8 Anchor features: **a** EM12; **b** damper device for EQRod1.1; **c** EQRod1.1 installed; **d** damper + cone device for EQRod1.2; **e** EQRod1.2 installed; **f** sleeved anchors SM10 and SM16

Table 2 Summary of anchor dimensions and shear resistances

Anchor	Type	Diameter (mm)	h_{eff} (mm)	$V_{n,stat}$ (kN)	$V_{n,seis}$ (kN)
EM12	Expansion	12	70	23.6	11.0
EQRod1.1	Expansion with damper	12	70	23.6	11.0
EQRod1.2	Expansion with damper and cone	12	70	23.6	11.0
SM10	Sleeved	8	50	13.1	6.6[a]
SM16	Sleeved	13	105	27.0[b]	13.5[a]

[a]There is no official seismic approval for this anchor and its seismic resistance is calculated as 0.5 times the static resistance

[b]The static resistance was calculated as the smallest of the values registered in the cyclic quasi-static experiments (Fig. 9)

Table 3 Calibration parameters of FR for each anchor type (see Fig. 7b)

Anchor	k_0 (kN/mm)	γ	d_{g0} (mm)	ΔF	α_0	α_1	α_2	α_3	β_0	β_1	β_2	β_3
EM12	0.40	0.38	2.20	0.8	0.15	1.0	0.50	2.20	30.5	42.0	25	0.10
EQRod1.1	0.40	0.38	1.50	0.8	0.05	1.0	0.40	2.00	14.2	22.5	17.3	0.16
EQRod1.2	0.40	0.88	0.50	0.8	0.15	0.9	0.40	1.50	7.3	4.0	4.0	0.10
SM16	0.40	1.88	0.25	0.6	0.00	0.5	0.10	1.50	30.0	25.0	20.0	0.11
SM10	0.60	0.67	0.25	0.8	0.00	0.9	0.25	1.50	10.0	12.0	7.0	0.20

loading via a rigid fixture (Quintana Gallo et al. 2019). Table 3 summarizes the calibration parameters of FR for each anchor. Figure 9 shows a comparison of the experimental and numerical hysteresis loops for the five anchor types.

5.2 Nonstructural component characteristics

The engine of an elevator, such as the one presented in Fig. 1c, is selected as the reference NSC case. This is needed to define the factors which depend on the specific NSC whose fixture and anchorage is being designed (importance/risk and performance/behaviour

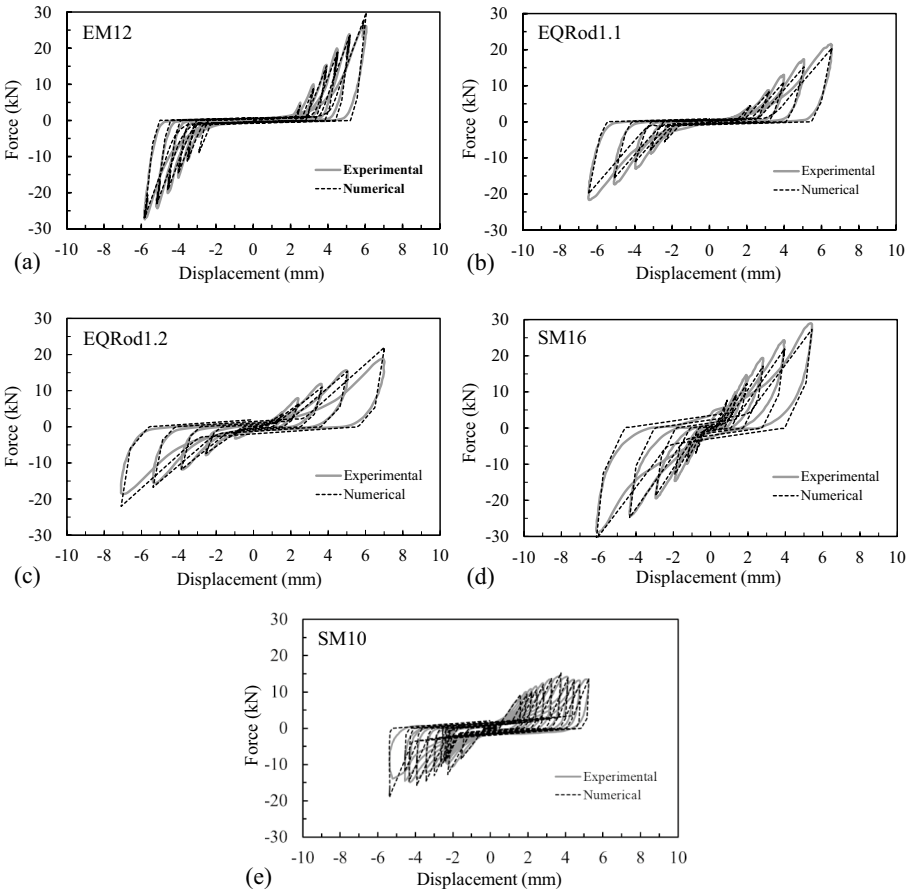

Fig. 9 Numerical-Experimental comparison and calibration of FR parameters: **a** EM12; **b** EQRod1.1; **c** EQRod1.2; **d** SM16; **e** SM10

factors). The mass of the NSC was defined by equating the design external force required by the New Zealand standard NZS1170.5 with the reduced nominal seismic shear strength of the anchor ($M_{NSC}=\phi V_{n,seis}/(c_{NZS}\ g)$). To define M_{NSC}, it was further assumed that the NSC was placed at the top storey of the host structure, because it is the most demanding case. The importance and performance factors were taken as $I_{NSC}=1.0$ and $S_{NSC}=1.0$, respectively, as required by the New Zealand code for the engine considered. Two values of the mass were considered for all the anchor cases, each of them defined with $V_{n,seis}$ of the anchors EM12 and SM10. Taking a strength reduction factor $\phi=0.75$, as required by NZS3101:2006 (Standards New Zealand 2006), and the values of $V_{n,seis}$ in Table 2, these two masses correspond to $M_{NSC,1}=0.20$ ton and $M_{NSC,2}=0.375$ ton.

Even though the fixture is assumed to be fully rigid (such as the base plate of the engine shown in Fig. 1b), the anchorage, as considered herein, provides flexibility to the NSC single degree of freedom (SDOF) system. For example, an initial elastic period of the NSC can be estimated using the initial stiffness of the FR model, k_0, which for all anchor cases except for SM10, is equal to 0.4 kN/mm ($k_0=0.6$ kN/mm for the anchor SM10).

Alternatively, the effective stiffness of the slippage region, $k_s = \gamma k_0$ could be considered (γ given in Table 3 for each anchorage case). Furthermore, an effective secant stiffness from the origin to a given maximum displacement and force could be selected (see Pürgstaller et al. 2020). Nevertheless, it is argued that this computation is more guesswork than a meaningful exercise. It is argued that none of these initial periods might provide a reliable source for anticipating the response of the NSC, whose anchorage behaviour is highly non-linear.

6 Input motions

The input motions correspond to a suit of 40 records, including 20 near-fault and 20 far-field events (a combination of the motions used in Pürgstaller 2017; Rojas (2020), and Bianchi et al. (2021)) (Table 4). The ground motion records were modified following the scaling procedure provided by the New Zealand standard NZS1170.5. That is, determining the k_1 scale factor that minimizes in a least mean square sense the difference between the ground motion spectra and design spectra at Ultimate Limit State (ULS) for the entire range of periods of interest. Figure 10 presents the pseudo-acceleration response spectra of the individual records with their average value, and the design spectra of both the standards NCh433 and NZS1170.5, for the site conditions defined in the problem.

7 Results and discussion

The results of the numerical analyses are divided into those of the NSC and of the anchor itself. The first ones include: (1) the peak component acceleration amplification factor (PCAAF = PCA/PGA); (2) the component-to-floor amplification factor (a_p = PCA/PFA); (3) the peak component absolute acceleration (PCA); (4) the peak component-to-floor relative displacement (PCRD); and (5) the peak component-to-floor relative velocity (PCRV). For the anchors, in turn, the results include the peak anchor force in absolute terms (F_A^{max}). The NSC results are compared to the corresponding values required by the code provisions reviewed, whereas the anchor results are also compared against $V_{n,seis}$ of each anchor type.

The results of the NSC and anchor are combined by plotting the PCRV versus F_A^{max} for each anchor type, input motion, and mass case, showing that there is a direct relationship between these two variables. This relationship is depicted in deeper detail using a novel three-dimensional (3D) graph which shows the evolution in time of the vector $L(t) = [F_A(t), v_{NSC}(t), d_{NSC}(t)]$ for two selected cases ($v_{NSC}(t)$ and $d_{NSC}(t)$ are the relative to the floor velocity and displacement time-history responses of the NSC, and $F_A(t)$ is the anchor force time-history response). The 3D plots are presented alongside three two-dimensional graphs, each of them corresponding to one of the three orthogonal projections of $L(t)$ in the three orthogonal principal planes.

7.1 Nonstructural component response

Figure 11 presents the values of the peak component acceleration amplification factor, PCAAF, obtained at each storey level of the building for all of the anchor types, earthquake records, and mass cases. These overall results of PCAAF present a large scatter (see

Table 4 Summary of earthquake ground motions

Event	Year	M_w	Station	Original PGA (g)	Scaled PGA (g)	Record ID
Cape Mendocino	1992	7.0	Eureka- Myrtle & West	0.15	0.42	FF01
				0.18	0.37	FF02
Landers	1992	7.3	Morongo Valley	0.19	0.36	FF03
				0.14	0.24	FF04
Landers	1992	7.3	North Palm Spring	0.14	0.41	FF05
				0.13	0.33	FF06
Landers	1992	7.3	Palm Springs Airport	0.08	0.23	FF07
				0.09	0.25	FF08
Hector Mine	1999	7.1	Amboy	0.18	0.39	FF09
				0.15	0.35	FF10
Friuli	1976	6.0	ST33	0.11	0.33	FF11
				0.09	0.29	FF12
Umbria-Marche	1997	6.0	ST223	0.17	0.46	FF13
				0.11	0.32	FF14
Darfield	2010	7.1	Christchurch Resthaven	0.24	0.30	FF15
Imperial Valley-06	1979	6.5	El Centro Array #4	0.48	0.49	NF01
				0.36	0.43	NF02
Imperial Valley-06	1979	6.5	El Centro Array #7	0.34	0.31	NF03
				0.46	0.33	NF04
Imperial Valley-06	1979	6.5	El Centro Differential Array	0.35	0.54	NF05
				0.48	0.40	NF06
Superstition Hills-02	1987	6.5	El Centro Imperial County Centre	0.36	0.41	NF07
				0.26	0.46	NF08
Darfield	2010	7.1	Christchurch Hospital	0.20	0.29	NF09
Darfield	2010	7.1	Christchurch Cathedral College	0.24	0.32	NF10
Christchurch	2011	6.3	Christchurch Resthaven	0.38	0.23	NF11
Christchurch	2011	6.3	Christchurch Hospital	0.34	0.3	NF12
Christchurch	2011	6.3	Christchurch Cathedral College	0.35	0.25	NF13
Christchurch	2011	6.3	Christchurch Botanic Gardens	0.57	0.38	NF14
				0.42	0.46	NF15
Christchurch	2011	6.3	Christchurch Botanic Gardens	0.53	0.53	EQ1
Christchurch	2011	6.3	Christchurch Cathedral College	0.36	0.36	EQ2
Christchurch	2011	6.3	Christchurch Hospital	0.71	0.71	EQ3
Christchurch	2011	6.3	Christchurch Resthaven	0.48	0.48	EQ4
Maule	2010	8.8	Concepción Centro	0.47	0.47	EQ5
				0.34	0.34	EQ6
Viña del Mar	2010	8.8	Viña del Mar Marga Marga	0.34	0.34	EQ7
Michoacán	1985	8.1	Secretaria de Comunicaciones y Transportes	0.17	0.17	EQ8
Kobe	1995	6.9	Japan Meteorological Centre	0.84	0.84	EQ9
Valparaíso	1985	8.0	Viña del Mar Marga Marga	0.36	0.36	EQ10

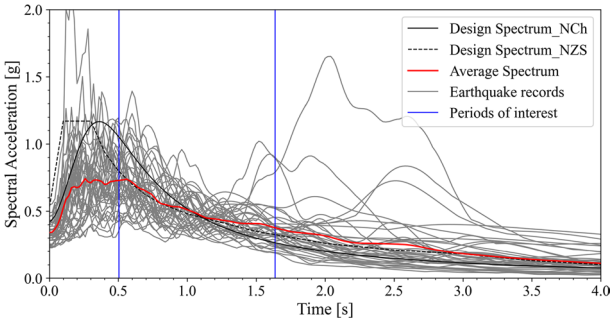

Fig. 10 Input motion response spectra

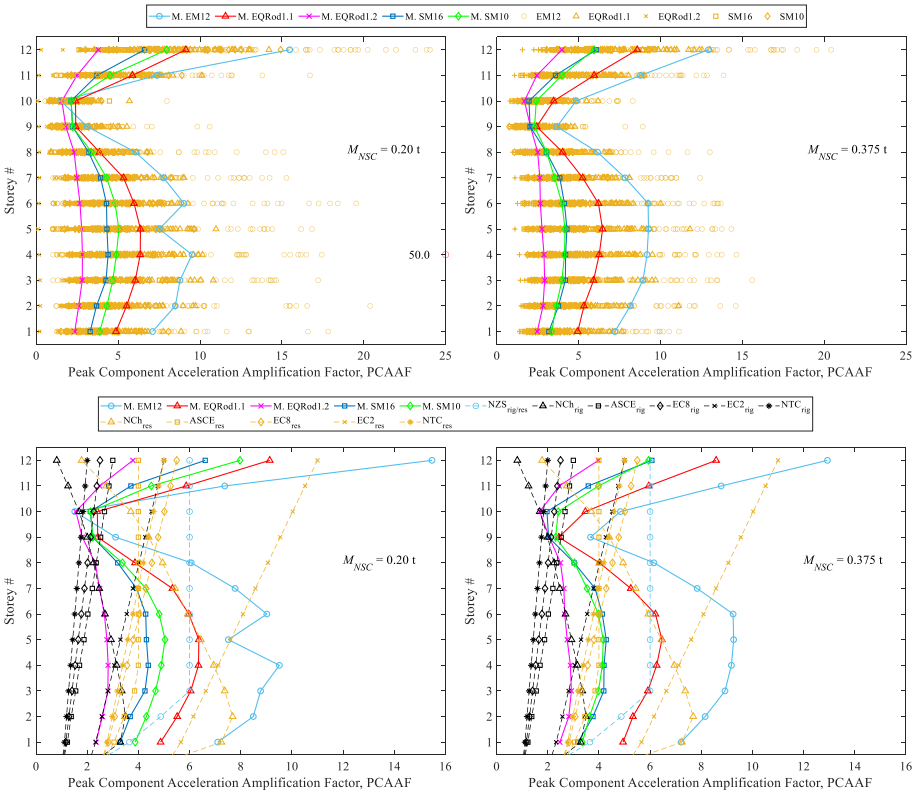

Fig. 11 PCAAF, all anchor cases (*Note* M. stands for 'mean')

Fig. 13, presented later, for a quantification of the data dispersion), with many cases largely exceeding the mean values of each anchor case, shown with the solid lines. The results obtained with the two different masses do not appear to be greatly different from each other. Even though it is difficult to distinguish between anchor types in Fig. 11, it can be observed that the largest values of PCAAF are predicted for the anchor EM12.

Figure 11 shows that, for most of the storey levels, the greatest mean values of PCAAF were obtained for the anchor cases EM12 and EQRod1.1, in that order, whereas

the smallest were obtained with the anchor EQRod1.2. The sleeved anchors SM16 and SM10 presented similar mean values of PCAAF, which for most of the storey levels were larger than those of EQRod1.2, but smaller than EQRod1.1. In addition, Fig. 11 shows that most of the values of PCAAF obtained with the seismic prescriptions surveyed greatly underestimate the numerical results (individual and mean values), except for EC2 for the resonance case (note this code included the annular gap factor, α_{gap}), and, to a lesser extent, NZS (for the identical cases of resonance and rigid fixtures) and NCh (resonance case with the additional factor of A = 2.0). One can notice, however, that the very small values of PCAAF required by NCh for the upper storeys are not in line with, when not significantly far from, the numerical results as well as with the prescriptions of all the other codes. The codes NTC, EC8, and ASCE (resonance case), and EC2 (rigid fixture case), in turn, appear to provide conservative values only with respect to the mean values obtained for the anchor EQRod1.2. Nevertheless, as mentioned before, the mean values of the results are exceeded in several cases, and sometimes by a large extent. Thus, arguably, the code approaches might not necessarily guarantee an acceptable level of performance-safety control.

To better understand and visualize the contribution of each anchor type to the results presented in Figs. 11, 12 presents box-charts of PCAAF for each anchor type and mass case separately. Each of these boxplots (presented in black) provides the median, the 25th and 75th percentiles, and the minimum and maximum (extreme) values of the data examined, for a set of different categories, such as storey level in this case. Figure 12 also shows the mean average values of each of the data sets (blue line with circular markers), and the code provisions for rigid fixtures (orange lines), for flexible fixtures at resonance (violet lines), and for the particular case of NZS (light blue line). Figure 12 also provides the 95th percentile of the data at each storey level (denoted P95; purple line with diamond markers). P95 is the value of PCAAF (in this case) that is exceeded only in 5% of the total number of cases. As in this case there are 40 results per floor, there are only two cases that exceed P95 at each storey, and there is only one result falling between the maximum extreme value and P95. Defining what would be an acceptable number of exceeding cases is beyond the scope of this work, but deals with non-epistemic values: societal, political, ethical (Rudner 1953; Douglas 2010; also see Quintana Gallo and Carradine 2021), related to the danger involved in the consequences of being wrong: number of un-safe cases accepted (Rudner 1953). However, a 5% exceedance could be considered a reasonable limit, similar to that for the characteristic compression strength of the concrete, for instance, and is herein proposed to be considered for a more rational approach to the problem compared to the mean values, acknowledging that it cannot be defined based on technical considerations, but rather on consensus (Quintana Gallo and Carradine 2021).

Figure 12 shows with much more clarity that the predicted values of PCAAF: (a) presented the greatest magnitude and scatter for EM12, followed by EQRod1.1; (b) are the smallest and less disperse for EQRod1.2, while a large dispersion is found for EM12 (see Fig. 13); and (c) do not vary significantly for the two mass cases, except for EM12, where they are relatively larger for M_{NSC} = 0.2 t compared to M_{NSC} = 0.375 t. Particularly great values of PCAAF with important scatter levels were obtained for EM12 (PCAAF = 50 for storey #4), such that none of the code provisions provide conservative estimations of even the mean and median of the numerical results (except for storey #10). The values of P95 exceed the code prescriptions by a large extent. In the case of EQRod1.2, the provisions of EC2 are conservative in all the cases. For SM16 and SM10, in turn, they are conservative with respect to P95, meaning that the prescriptions of EC2 are exceeded in only a few of the cases. All the other code provisions for rigid fixtured NSC underestimate the results

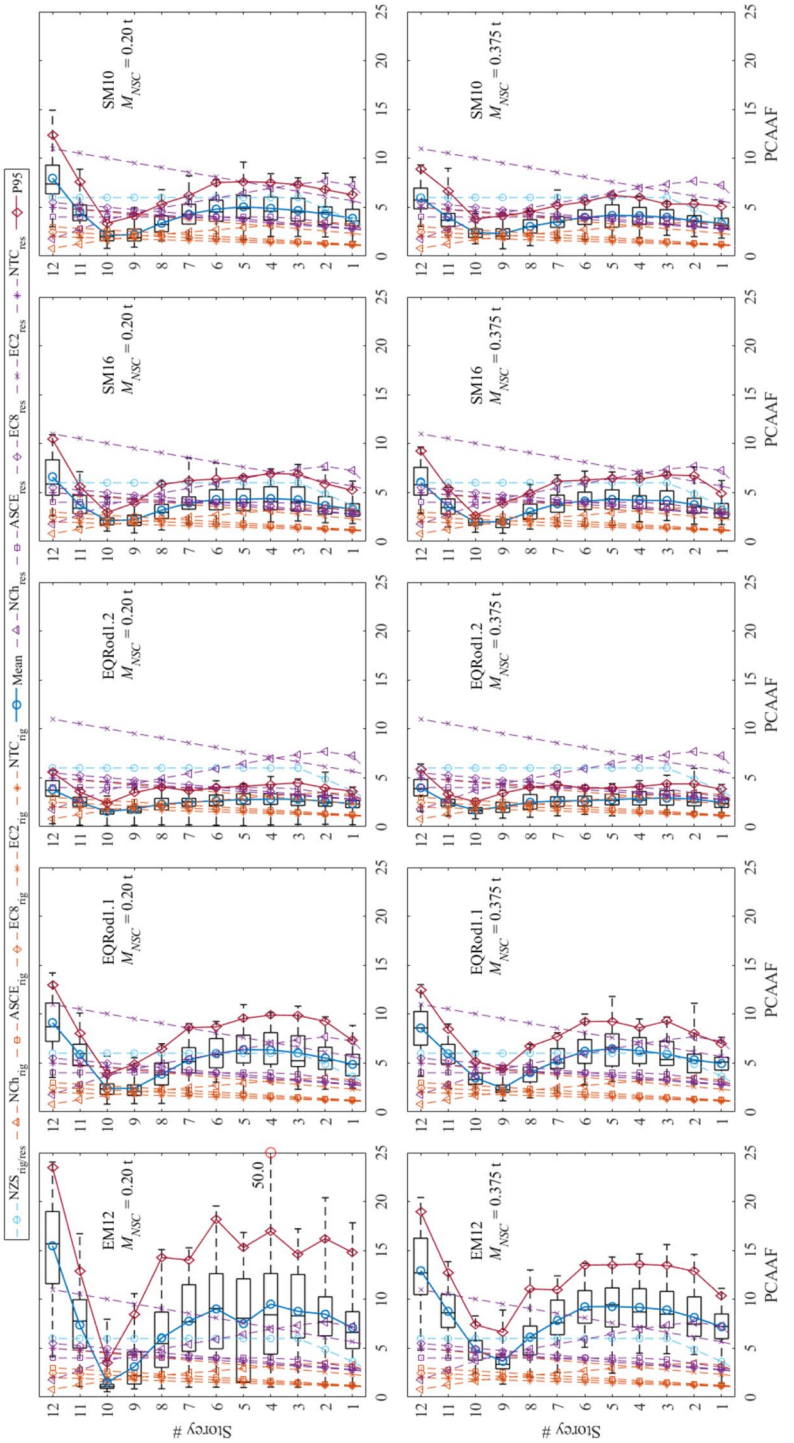

Fig. 12 Peak Component Acceleration Amplification Factor, PCAAF = PCA/PGA, all cases

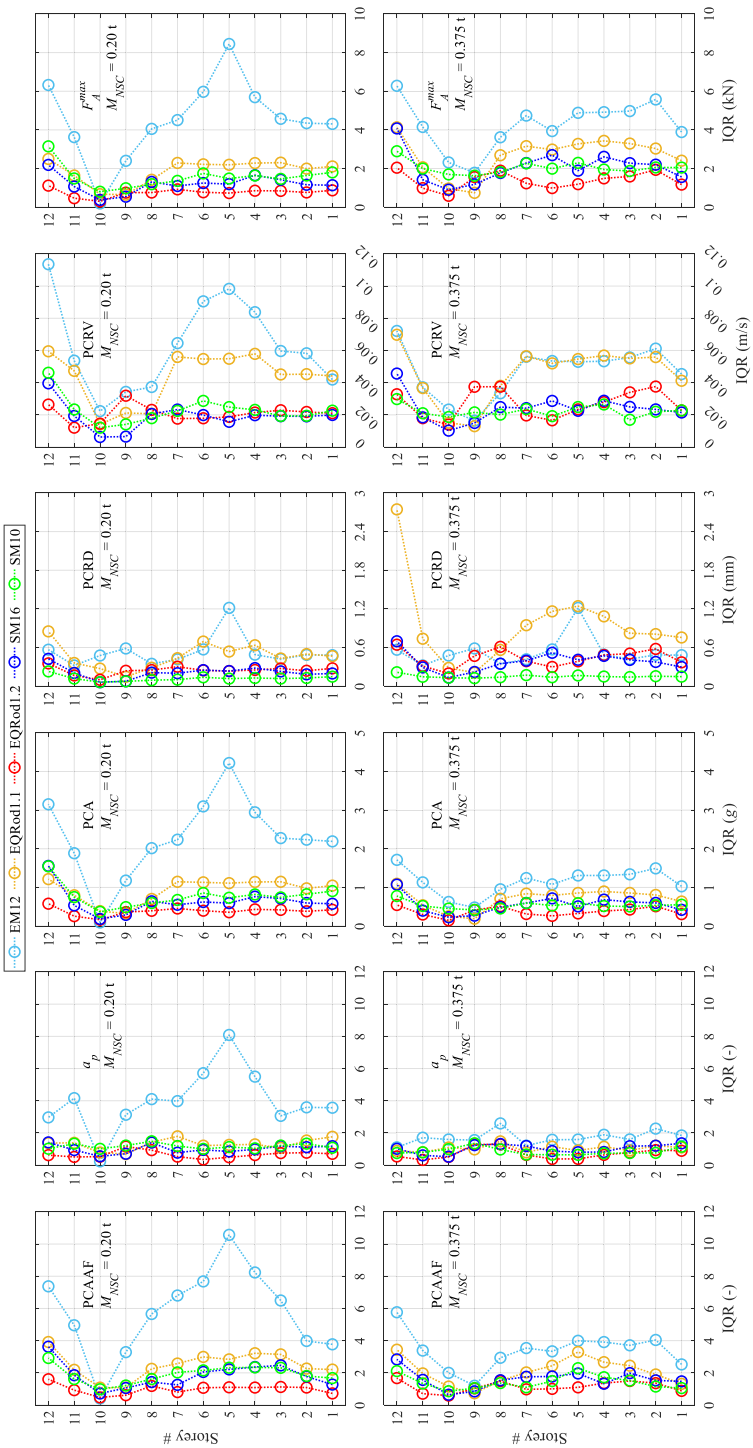

Fig. 13 Measurement of scatter in results: Inter-quartile range (IQR) all variables examined

obtained with all of the anchor types, implying that the assumption of full rigidity does not appear to be adequate when the anchorage hysteresis is considered and there is no mortar filling the annular gap (Ciurlanti et al. 2022).

To provide a quantification of the scatter encountered in the results, Fig. 13 presents the inter-quartile range (IQR) of PCAAF (first column), as well as of the other variables revised later in the paper. The IQR dispersion index corresponds to the difference between the values of the 75th and 25th percentiles of the data at each storey level and is measured in the units of the evaluated variable (i.e., for PCAAF, IQR is dimensionless). It seems clear from the first column of graphs of Fig. 13 that the largest and smallest IQR are presented by EM12 and EQRod1.2, respectively, for almost all the storey levels (IQR < 2.0 for EQRod1.2). The value of IQR for EM12 is particularly large for $M_{NSC} = 0.20$ t, reaching up to IQR ≈ 11. To distinguish between the relative contribution to PCAAF of the floor acceleration and the floor-to-component amplification (PFA and a_p, respectively), Fig. 14 presents, for all the input motions and at each storey level, the values of: (a) the peak floor-to-ground acceleration amplification factor PFAAF = PFA/PGA, and (b) a_p, for all the anchor types, and the two mass cases. The figure shows a considerable scatter in the magnitude of PFAAF depending on the input motion, for all the storeys. Figure 14 shows that large values of PFAAF are predicted, in some of the cases, independently of the storey level. Therefore, it is not always true that larger PFA occur at the upper storeys compared to the bottom ones as assumed by most of the code provisions. Most of the values of PFAAF were smaller than 2.0, and all of them were smaller than 3.0. Comparing the numerical vs. analytical code results, Fig. 14 shows that: (a) NZS provides the most assertive recommendation for PFAAF, at its prescription is greater than the maximum results obtained with the analyses for all the storey levels; (b) ASCE, EC8, EC2, and NTC formulations are exceeded in a limited number of cases and are greater than the average value of PFAAF at all the storey levels; and (c) the prescribed values of PFAAF by NCh are exceeded in several cases, particularly in the upper storeys (always exceeded in the top storey level).

The results of a_p depicted in Fig. 14 present large scatter, particularly for the smallest M_{NSC} (see Fig. 13). As also found for PCAAF, the mean values of a_p predicted for EQRod1.2, followed by SM16 and SM10, are smaller than those obtained with EQRod1.1 and EM12 (EM12 presents the greatest mean values of all the anchor cases). Figure 14 also shows that, in a considerable number of cases, the code provisions surveyed prescribe smaller values of a_p compared to those predicted numerically, taking all the anchor cases into account. In fact, all the codes underestimate even the mean values of a_p obtained for the anchor case EM12 for most of the storey levels, as well as for EQRod1.1 for some of them (both mass cases). In terms of mean values, the results obtained for all the anchor cases are underestimated by all the code recommendations for rigid fixtures (both mass cases). This is also true for NZS at resonance, as, according to this standard, a_p is the same for rigid and flexible fixtures at resonance. In the light of the overall results obtained for PCAAF, PFAAF and a_p, it can be concluded that, in a general sense, the code prescriptions underestimate the component-to-floor acceleration amplification of the NSC, probably because they neglect the effect of the anchorage hysteresis, whereas they recommend rather adequate values for the floor-to-ground magnification of the acceleration.

Figure 15 presents the same type of graphs shown Fig. 12, but for a_p = PCA/PFA. This figure reflects the same scenario presented for PCAAF, with the largest magnitude and variability of the a_p results obtained for EM12 compared to the rest of the anchor cases. According to Fig. 13, IQR of EM12 for $M_{NSC} = 0.20$ t is much larger than for all the other anchor cases (IQR up to 8). For $M_{NSC} = 0.375$ t, on the other hand, IQR is larger for EM12 than for the other anchor cases, but not by a significant extent. For all the anchor cases,

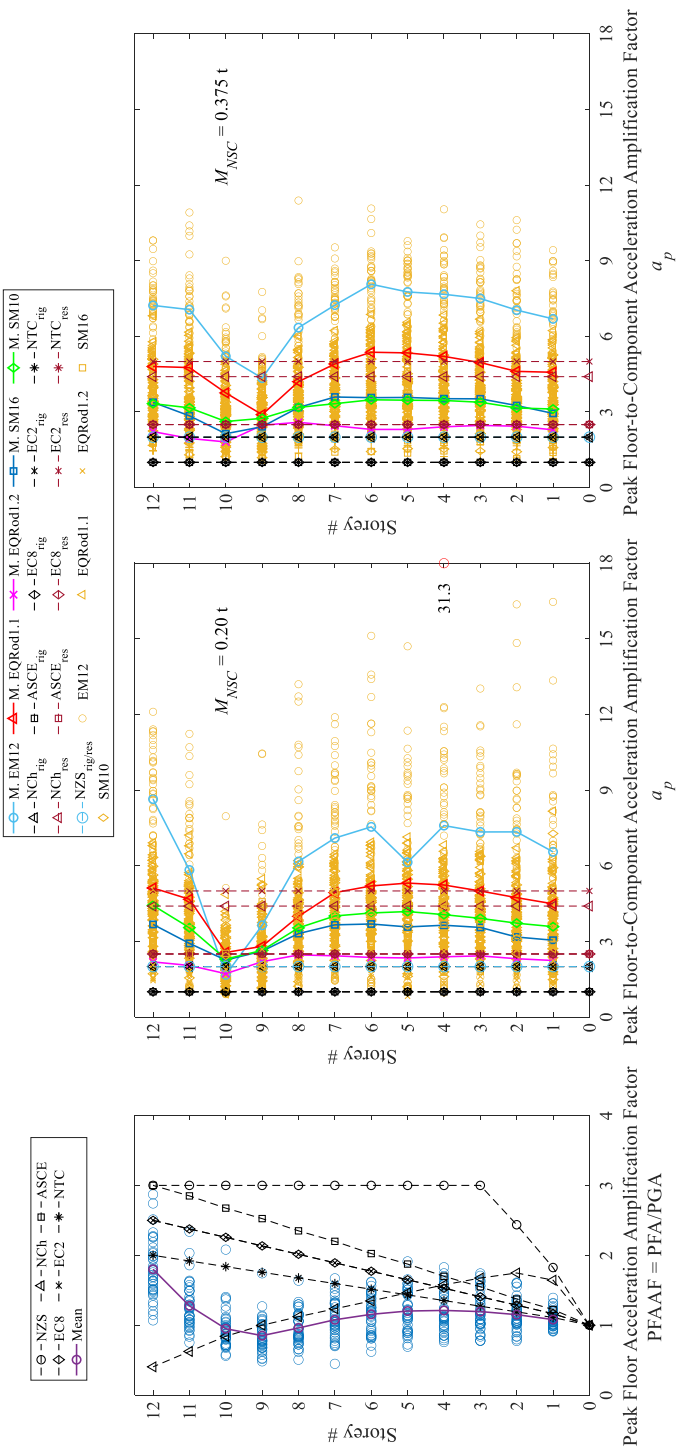

Fig. 14 PFAAF and a_p, all anchor cases (*Note* M. stands for 'mean')

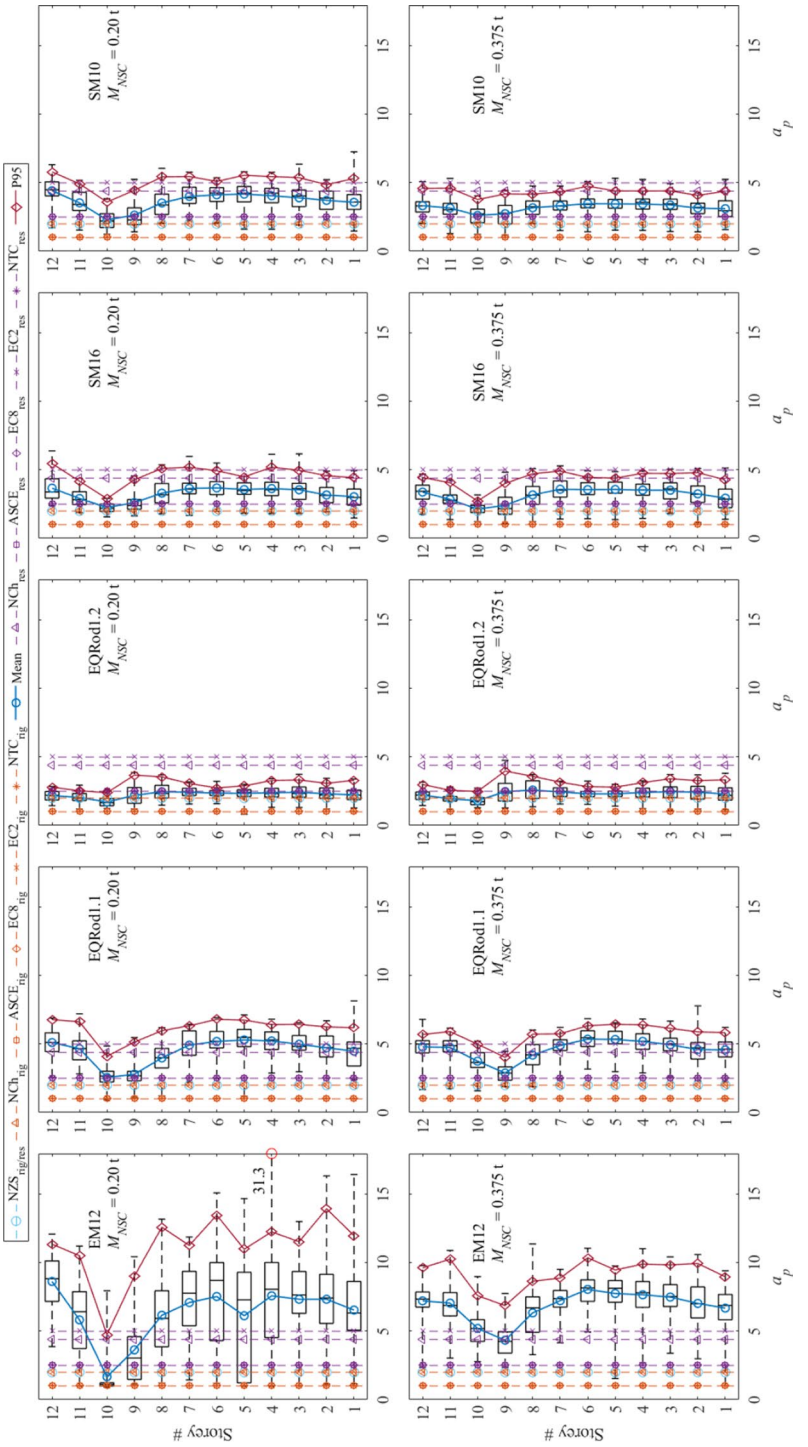

Fig. 15 Component-to-Floor Acceleration Amplification Factor, a_p = PCA/PFA all cases

Fig. 15 shows that the mean values of a_p ($a_p{}^{\mathrm{M}}$) obtained for all the anchor cases are larger than those prescribed by all the code provisions for NSC with rigid fixtures. For NSC with flexible fixture at resonance, NCh and EC2 provide conservative estimations of $a_p{}^{\mathrm{M}}$ at most of the storey levels for the anchor cases EQRod1.2, SM16 and SM10 (both mass cases), but are smaller than the P95 values for SM16 and SM10 in some of the storey levels. Overall, the anchor with the best performance (lowest values of a_p) is EQRod1.2 closely followed by SM16 and SM10.

To analyse the maximum acceleration of the NSC in absolute terms, Fig. 16 provides the previously presented statistical evaluation, but for PCA. The figure also provides the values of PCA computed as $\mathrm{PCA}=F_{NSC}/W_{NSC}$ (in units of g) according to the different code provisions reviewed (Sect. 3). These graphs are needed because, at least theoretically, a large PGA can lead to moderate PCA values, and a small PGA may lead to rather large PCA values. Hence, it is not necessarily true that large PCAAF imply large PCA and vice versa. Figure 16 shows, nonetheless, that a similar trend compared to PCAAF is found for PCA, such that the largest component accelerations are found for EM12 and the smallest for EQRod1.2 and so forth. Again, the prescriptions by EC2 are always conservative only in the case of EQRod1.2, and all of the other code provisions are unconservative in all of the anchor cases. Very large PCA values are found for EM12 in some of the cases, which could be excessive for any NSC. Figure 16 also shows that the PCA is predicted to have similar values at all the storey levels. This appears to be in contradiction with the prescription of PCA proportional to the vertical location of the NSC in the host structure (Sect. 3.3), as it is done by all of the code provisions reviewed, except for NZS.

Figure 17 presents the statistical analysis of PCRD for all the anchor and mass cases. Note that the revised codes do not provide limits for PCRD, even though excessive displacements can be detrimental for some NSC and anchors. Figure 17 shows that, overall, the results for PCRD presented less dispersion than PCAAF, a_p, and PCA. Most of the predicted values of PCRD are contained within a narrow band, depicted by the chart's boxes (percentiles 25 to 75), with the exception of EQRod1.1, for both mass cases, but particularly for $\mathrm{M}_{NSC}=0.375$ t. On average and in terms of P95, the largest PCRD were found for ERod1.1 and EM12, in that order, whereas the smallest were obtained for SM10. Figure 18 provides the statistical analysis of the PCRV results. Overall, Fig. 18 reflects the trends presented by PCA in Fig. 16 (magnitude and dispersion of the results), suggesting that there is a direct relationship between PCRV and PCA, and therefore $F_A{}^{max}$, as shown later on the paper. For instance, the exceptionally great values of PCA predicted for $\mathrm{M}_{NSC}=0.375$ t at storeys #4 and #6 are predicted for PCRV as well. Note that a large PCAAF is predicted for storey #4, but not for storey #6. No maximum value of PCRV is stipulated by the revised code prescriptions. Columns four and five of Fig. 13 present a quantification of the results' dispersion for PCRD and PCRV, respectively, showing that the largest IQR are obtained for EM12 and EQRod1.1. For PCRD and $M_{NSC}=0.375$ t, the results for EQRod1.1 present IQR $\approx$ 3 mm in the top storey, whereas for the rest of the cases IQR < 1.2 mm. For PCRV, on the other hand, the greatest values of IRQ are found for EM12 and $M_{NSC}=0.375$ t.

7.2 Anchorage response

For each mass case, Fig. 19 presents an analysis of the maximum anchor force ($F_A{}^{max}$) obtained for all anchor cases. The nominal shear strength of the anchors ($V_{n,seis}$) is also plotted in Fig. 19, for comparison (referred to as V_{n1} for EM12, EQRod1.1, and EQRod1.2; V_{n2} for SM16, and V_{n3} for SM10; Table 2). The graphs of Fig. 19

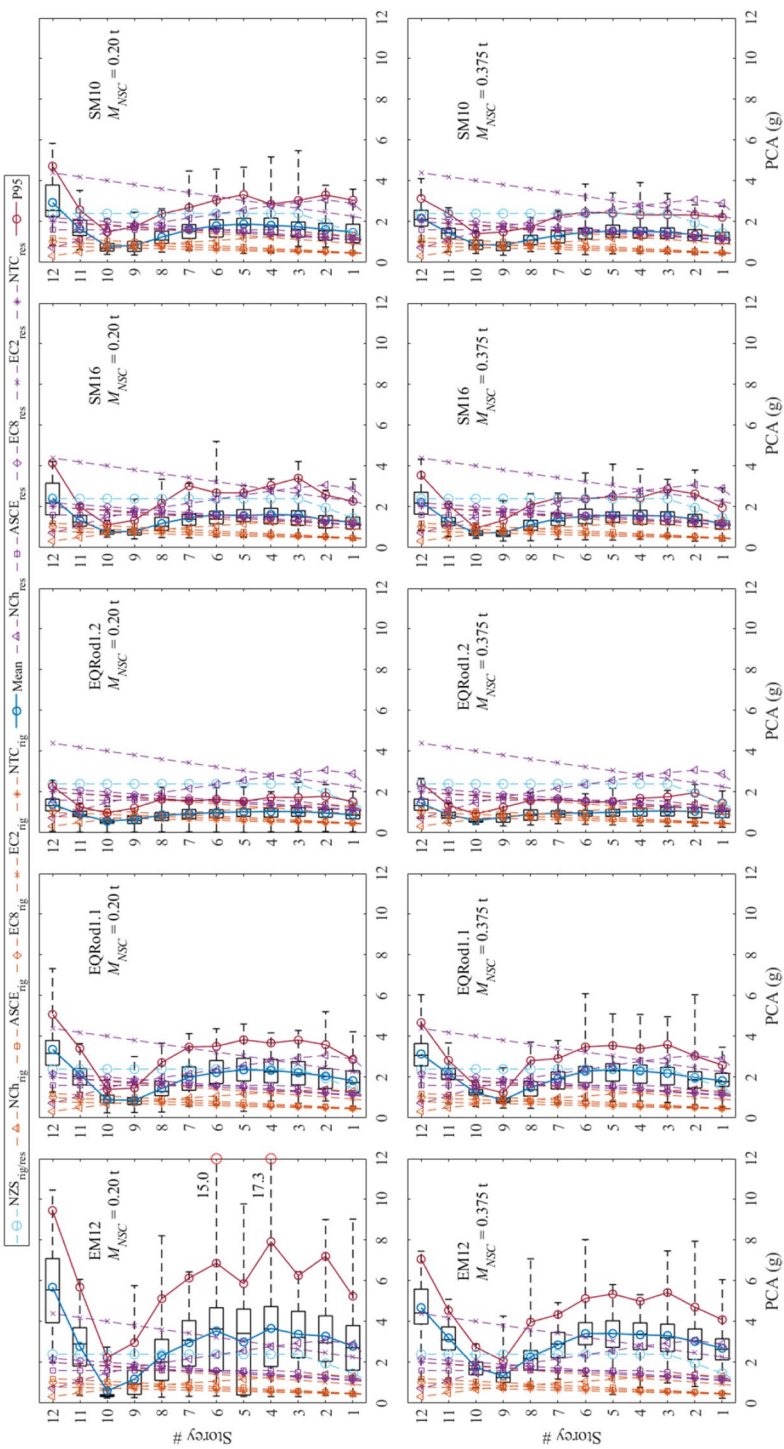

Fig. 16 Peak Component Acceleration, PCA, all cases

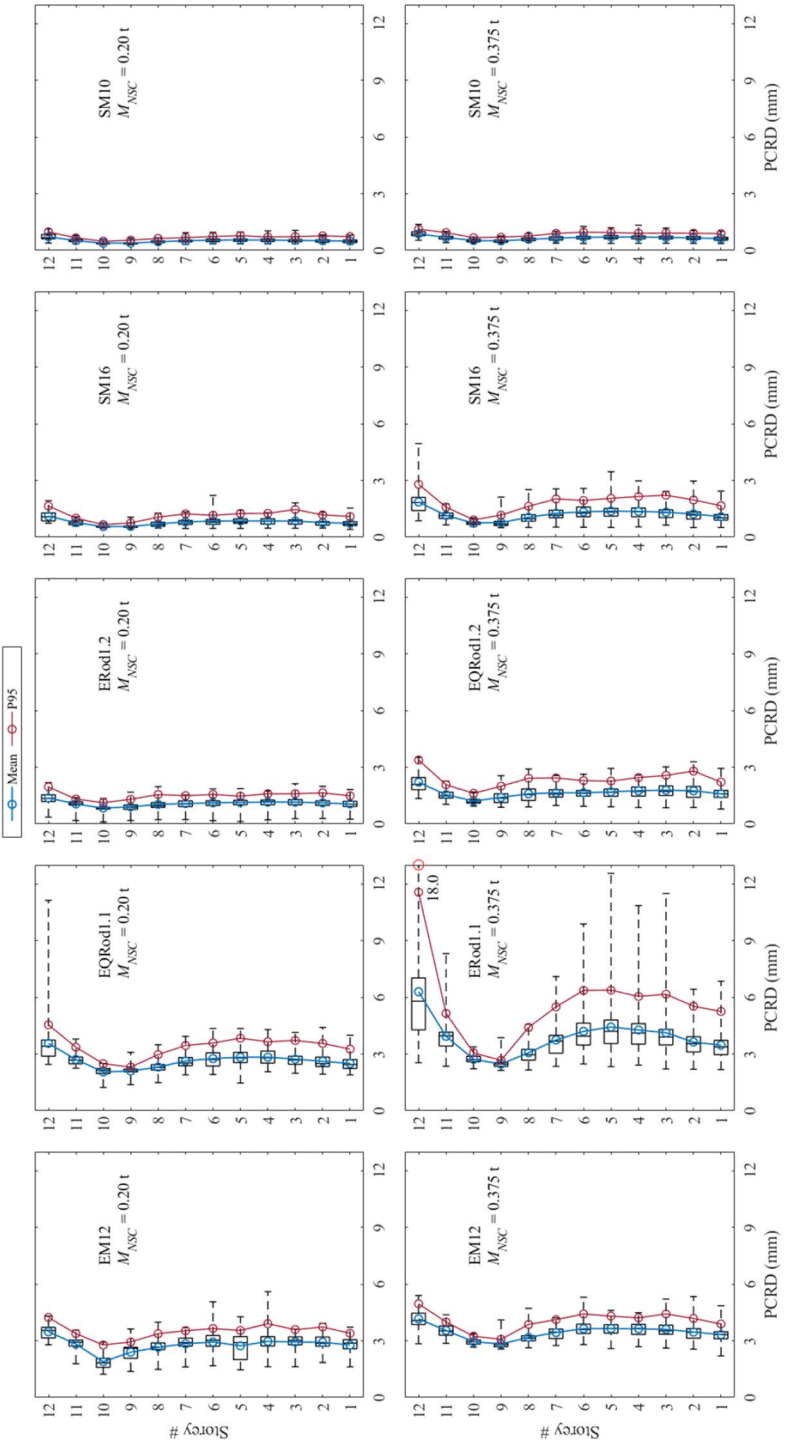

Fig. 17 Peak Component Relative Displacement, PCRD, all cases

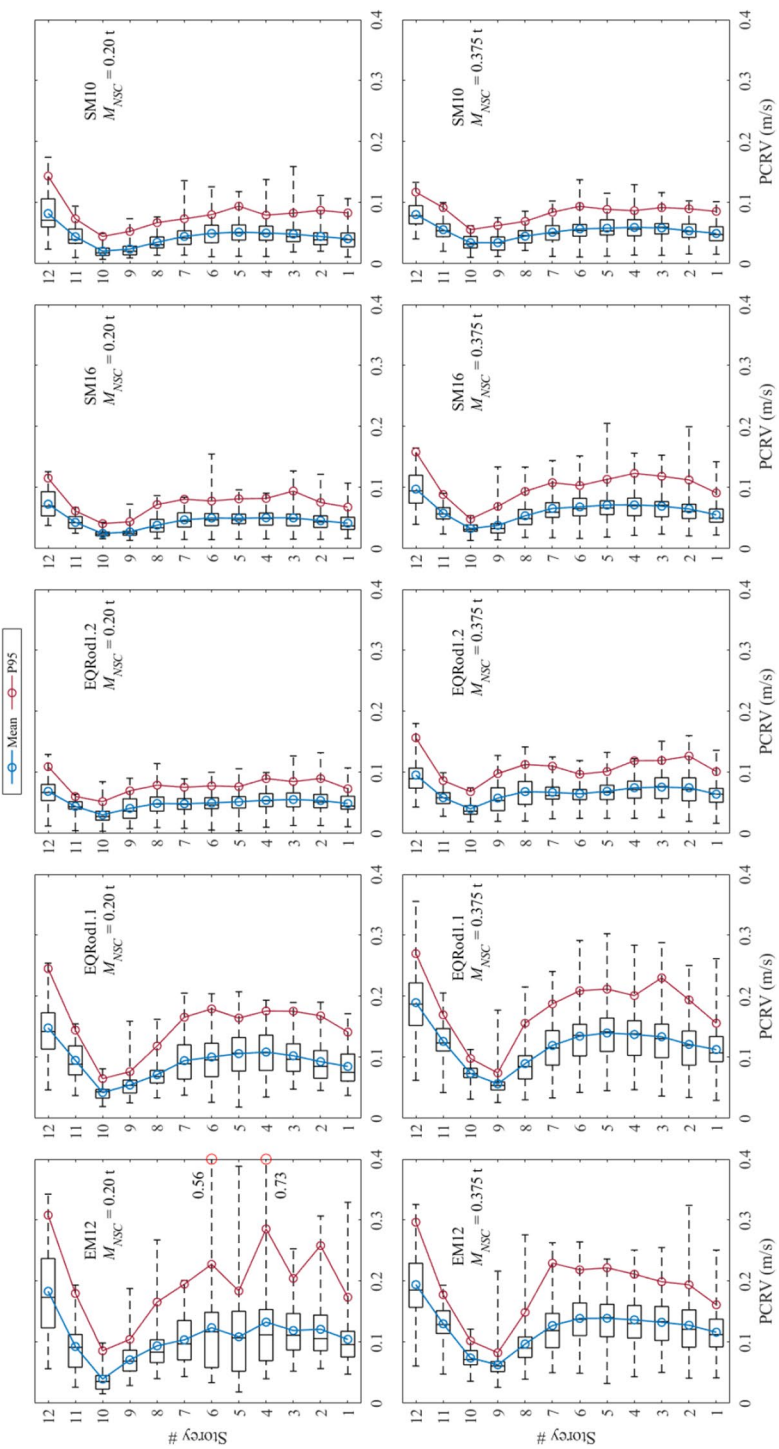

Fig. 18 Peak component relative velocity, PCRV, all cases

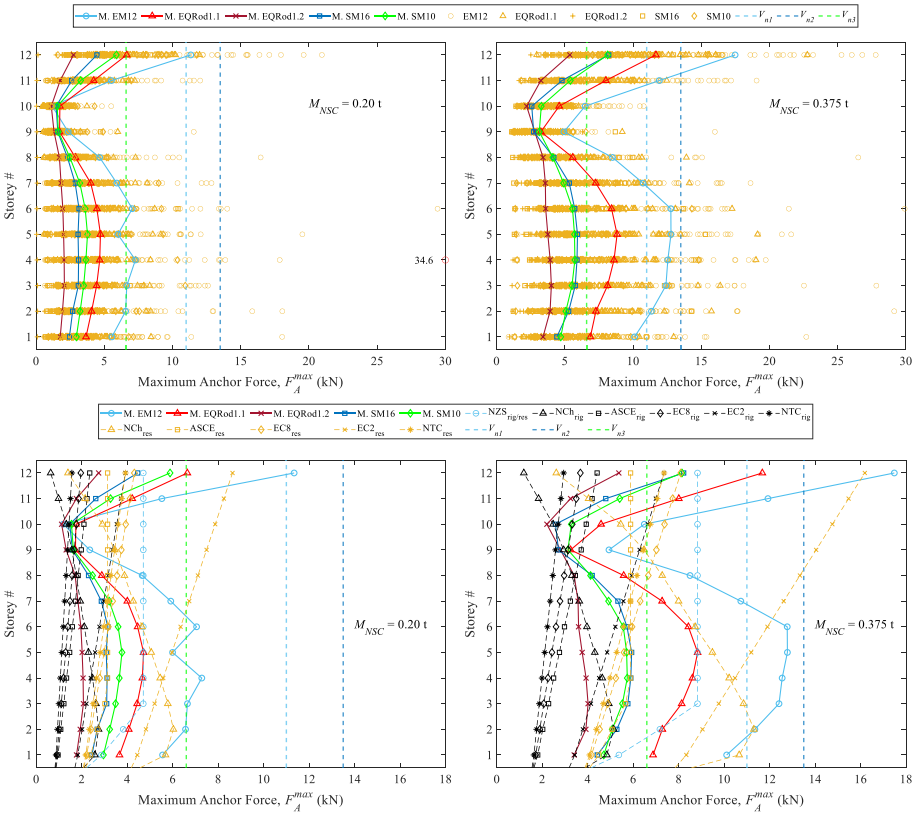

Fig. 19 Maximum anchor force F_A^{max}, all cases (*Note* M. stands for 'mean')

approximately reflect the results previously presented for PCAAF, such that the maximum anchor force results present great scatter (see column six of Fig. 13). In this case, nevertheless, the maximum anchor force obtained for the larger mass are greater than for the smaller one, as expected. For both mass cases, Fig. 19 shows that the greatest mean average values of F_A^{max} are obtained for EM12 followed by EQRod1.1, and both sleeved anchor cases (SM16 and SM10). The smallest mean values of F_A^{max}, in turn, are obtained with EQRod1.2. In addition, the differences between such mean maximum values are larger for $M_{NSC}=0.375$ t compared to $M_{NSC}=0.2$ t. Also in terms of mean average, in some of the storey levels F_A^{max} exceeds the nominal shear capacity of the anchor for EM12 and $M_{NSC}=0.375$ t, implying that the anchor design is not safe even on average. Even though the numerical results are larger than the nominal strength in some of the cases, it does not necessarily mean that the anchor would reach failure, because their nominal shear strength for seismic applications can be quite conservative. For instance, EM12 was able to resist shear forces in the order of 30 kN according to the cyclic experiments shown in Fig. 9, whereas $V_{n,seis}=11$ kN only (Table 2).

Regarding the code provisions for NSC rigid fixtures, Fig. 19 depicts that none of them seem to provide conservative estimates of the numerical results for both masses and all anchor cases. This is true even though the smallest mass was computed to satisfy

the strength requirements of the less resistant anchor SM10 ($(M_{NSC}=\phi V_{n,seis}/(c_{NZS}\ g)$) and the code NZS, which prescribes the largest demands for NSC with rigid fixtures from all the codes surveyed. The provisions for NSC with flexible fixture (resonance case) of all codes, except for EC2, are also smaller than the mean average value of F_A^{max} for all of the anchors, except for EQRod1.2.

Figure 20 presents the predicted values of F_A^{max} for each anchor and mass case separately and compares them with the corresponding nominal strength of each anchor. The figure shows that, from all the anchor cases, EM12 presents: (a) the greatest magnitude of F_A^{max}; (b) the largest dispersion in the results (IQR > 4 kN in several storeys for both mass cases; see Fig. 13); (c) greater average vales of F_A^{max} compared to $V_{n,seis}$ for $M_{NSC}=0.375$ t; (d) greater P95 values of F_A^{max} compared to $V_{n,seis}$ for both mass cases; and (e) some particularly large forces (up to 34.6 kN), which greatly exceed the nominal seismic shear strength, and may imply the theoretical failure of the anchorage. The anchors EQRod1.1 and SM10, in turn, also present considerable scatter in the results, but to a lesser extent compared to EM12 (IQR ≈ 3 in the worst case; see Fig. 13); the mean average values of F_A^{max} do not exceed $V_{n,seis}$ in none of the mass cases, whereas the P95 values, in turn, do exceed such nominal resistance, in some of the storey levels. The anchor cases which present the best performance of all in terms of F_A^{max} appear to be EQRod1.2 and SM16, in that order, because they are predicted to present $F_A^{max} < V_{n,seis}$ for most of the individual cases (in all of them in the case of EQRod1.2), as well as their mean average and P95 values. It is worth noting, however, that the strength of SM16 is slightly larger than the one of EQRod1.2, which would mean that the latter would present the best performance of all the anchor types. In addition, the hysteresis loops of EQRod1.2 present a larger area compared to SM16, which provide an enhanced energy dissipation capability.

8 Relationship between F_A^{max} and the NSC's relative velocity and displacement

This section draws a relationship between specific results for the NSC and anchor, in the light of the previously described findings, and discusses the potential reasons behind the better performance predicted for some of them. In Sect. 7.1 of the paper, it was mentioned that the PCRV apparently presented the same magnitude trends compared to F_A^{max}. To investigate such a finding, Fig. 21 plots PCRV against F_A^{max} for all the anchor and mass cases. Figure 21 shows that the maximum anchorage force, F_A^{max} is apparently directly proportional to PCRV, such that the greater the velocity reached by the NSC, the larger the force experienced by the anchor. Furthermore, this relationship seems to be approximately linear, particularly in the case of the three anchors which presented less scatter in the results (EQRod1.2, SM16 and SM10; see Fig. 13). This apparent relationship is found for both mass cases.

To deepen the investigation on the relationship between PCRV and F_A^{max}, a novel three-dimensional (3D) plot, referred to as $L(t)$, is developed in the following (Fig. 22). First, it is important to note that as the equation of motion of the single degree of freedom (SDOF) NSC system depends explicitly on the time, it is a 2D non-autonomous system (Quintana Gallo and Meneses 2021). Thus, any 2D plot of curves such as force versus displacement (hysteresis loops) is self-intersecting. If such a dynamical system is in turn described by a system of three variables, it becomes a 3D autonomous system and the 3D plots of such variables in time are not self-intersecting curves that can provide a much deeper insight

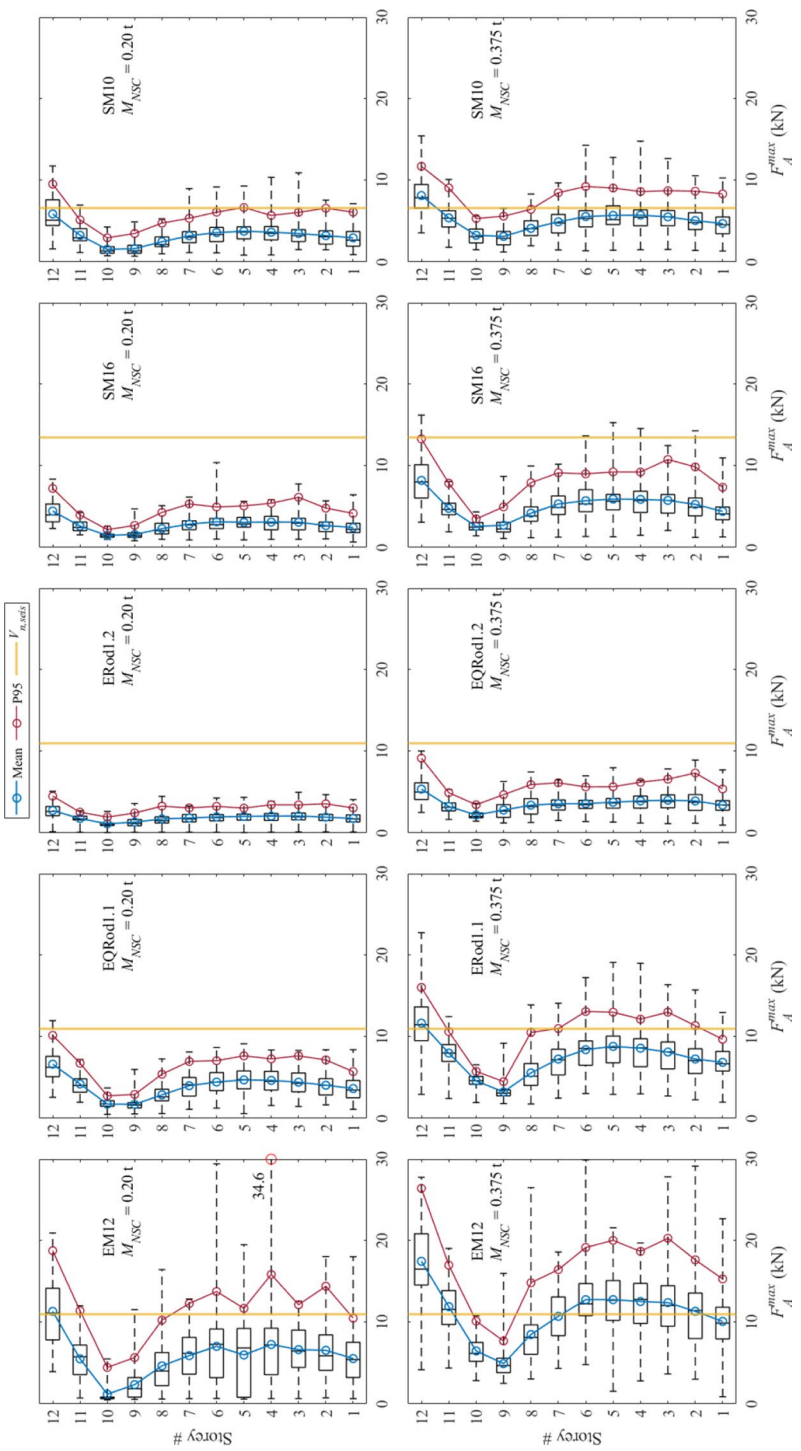

Fig. 20 Maximum Anchor Force, $F_A{}^{max}$, all cases

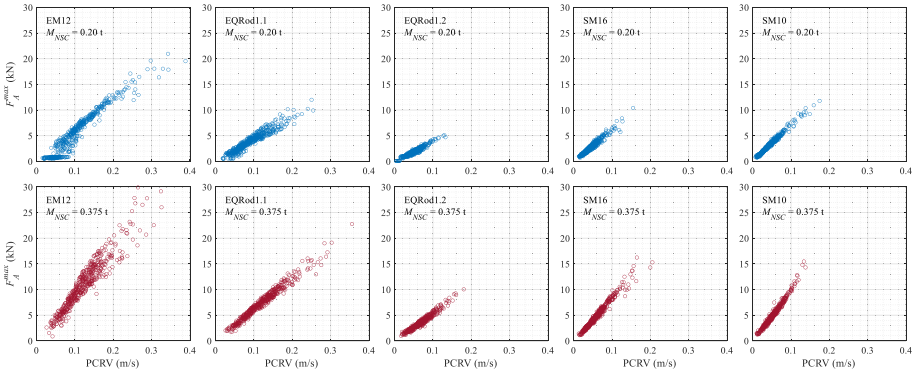

Fig. 21 Maximum anchor forces, F_A^{max}, versus peak component relative velocity, PCRV, all cases

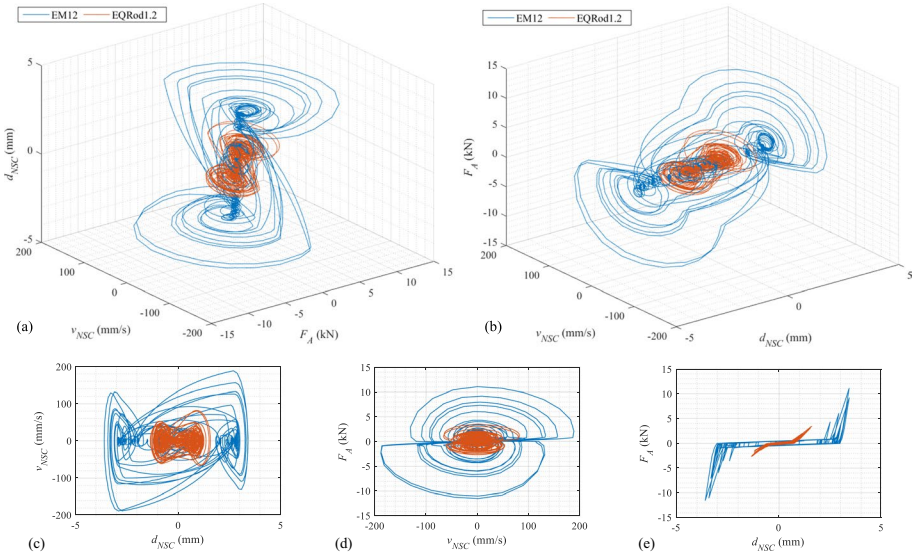

Fig. 22 Three-dimensional and two-dimensional curves of the NSC response (EM12 and EQRod1.2) (d_{NSC} = NSC's displacement relative to floor; v_{NSC} = NSC's velocity relative to floor; F_A = anchor's force): **a** $L(t)$ with d_{NSC} in vertical axis; **b** $L(t)$ with F_A in vertical axis; **c** $d_{NSC}(t)$ vs $v_{NSC}(t)$; **d** $v_{NSC}(t)$ vs $F_A(t)$; and **e** $d_{NSC}(t)$ vs $F_A(t)$

into its dynamics (Quintana Gallo and Meneses 2021). The novel 3D curve $L(t) = [d_A(t), v_{NSC}(t), F_A(t)]$, which describes the response of the NSC, and plotted apparently for the first time in this contribution, is not a self-intersecting curve that more clearly shows the relationship between $F_A(t)$ and $v_{NSC}(t)$, and also $d_{NSC}(t)$, in one single graph. Such a representation of the dynamics of the NSC is analogous to the classical 3D 'butterfly' curve encountered by Lorenz (1963) whilst modelling a meteorological phenomenon.

Figure 22 presents the $L(t)$ response of the fastener-NSC subsystem located at the structure's top-storey, for $M_{NSC} = 0.2$ t, the anchor EM12, and for one selected earthquake record. To better visualize it, the curve is plotted in two reference systems having the

displacement and force axes in the vertical position, respectively (Fig. 22a, b, respectively). In addition, Fig. 22 provides the following 2D plots: $d_{NSC}(t)$ vs $v_{NSC}(t)$ (Fig. 22c); $v_{NSC}(t)$ vs $F_A(t)$ (Fig. 22d); and $d_{NSC}(t)$ vs $F_A(t)$ (Fig. 22e), which correspond to the three orthogonal planes of the 3D figure on the right-had side of Fig. 22. The $L(t)$ curves show the following: (1) the velocity sharply increases when the anchorage is displaced from one loading end to the opposite; (2) in general, it appears that the larger the velocity reached in the gap region of the anchorage, the greater the force achieved during the loading state at the opposite end; (3) once the loading of the anchor against the concrete begins, the velocity is drastically reduced until it reaches a local maximum with the opposite sign and reduces following an spiral trajectory around the displacement axis; (4) the larger the gap size, the greater the magnitude of the velocity at the beginning of the anchor loading and thus the maximum force obtained.

Figure 22 shows that the magnitude of the $L(t)$ response for the anchor case EM12 is much greater than for EQRod1.2. This is thought to be the results of the greater gap of the anchorage of EM12 compared to EQRod1.2, which permits the development of larger velocities of the NSC and thus forces. In addition, the velocity vs force 2D graph depicts how for similar velocities at the start of loading, the maximum anchorage force achieved with EM12 is generally larger than with EQRod1.2, as a result of the smaller stiffness of the later anchorage. Lastly, it is clear from Fig. 21 that the force and displacement levels reached by EQRod1.2 are smaller compared to those obtained with EM12. As an appendix to the paper, an animation showing the evolution of $L(t)$ in time for EM12 (shown Fig. 22), is provided.

9 Summary and conclusions

In seismically active parts of the world, the damage suffered by nonstructural components (NSCs) during major earthquakes contributes with a large extent of the total economic losses produced by them. Currently, seismic codes worldwide do not forbid the occurrence of damage to NSCs during moderate and large intensity earthquakes. Nevertheless, as part of a modern damage-control design philosophy, it is desirable to limit the level of damage to both structural and non-structural parts of a building under any level of seismic intensity. Although current code provisions assume that there is full rigidity between the anchorage and the concrete and NSC's fixture, recent numerical work which included the shear hysteresis developed in the anchorage has shown that prescriptions following such assumption tend to be non-conservative when compared to those obtained through nonlinear dynamic analyses (NLDA). However, information about the effect of the type of shear hysteresis of the anchorage on the response of a NSC was not considered.

To fill such a research gap, this article presented a numerical study on the influence of the anchorage shear hysteresis on the seismic response of NSCs anchored to multi-storey reinforced concrete buildings, and of the anchorage itself. To cover different types of shear hysteresis shapes, this contribution considered the experimental results obtained for five types of post-installed fasteners (anchors). The results were used for calibrating the hysteresis model of the anchorage connecting a NSC with rigid fixture and a 12-storey RC building host-structure. Using a set of 40 ground motions and assuming a single NSC at each storey level anchored by a single fastener each, a series of NLDA of the structure-fastener-nonstructural (SFN) system was carried out.

The results showed significant differences in terms of maximum acceleration and force of the NSC and anchorage, respectively, depending on the type of anchor. These seismic demands were sometimes larger than those required by the reviewed code provisions for NSC with rigid fixture, but also for the most restrictive code prescriptions for flexible NSC (resonance case). The results presented different amounts of scatter, mostly related to the size of the annular gap and of the loading stiffness of the anchorage. The largest levels of dispersion of the results were found with the expansion anchor size M12, referred to as EM12. It was shown that the maximum force achieved by the anchorage is directly related to the peak relative-to-floor velocity of the NSC within the slip region, such that the smaller the annular gap, the smaller the relative velocity of the NSC and, therefore, the smaller the force to-be-resisted by the anchorage (force demand). It was concluded that the shape of the shear hysteresis of the anchorage highly influences the response of the NSC and the anchor itself and should not be neglected in practice. It was also concluded that, amongst the several anchorages studied, the anchors EM12 and EQRod1.2 (closely followed by the sleeved anchors) presented the less desirable and best performances of all, respectively.

Supplementary Information The online version contains supplementary material available at https://doi.org/10.1007/s10518-023-01642-w.

Author contributions DR: Conceptualization, Investigation, Formal analysis, Data curation, Writing—Review and Editing. PQG: Conceptualization, Investigation, Visualization, Supervision, Writing—Original Draft. AP, SB, JC, SP, KB: Conceptualization, Writing—Review and Editing.

Funding Open access publishing supported by the National Technical Library in Prague.

Declarations

Conflicts of interest There is no conflict of interest.

Ethics approval Not applicable.

Consent to participate All the authors agreed to participate in the writing of this manuscript.

Consent for publication All the authors agreed to submit this manuscript.

References

ACI Committee 318 (2005) ACI318M-05: building code requirements for structural concrete and commentary. American Concrete Institute, Farmington Hills

Adam C, Furtmuller T, Moschen L (2013) Floor response spectra for moderately heavy nonstructural elements attached to ductile frame structures. In: Papadrakakis M, Fragiadakis M, Plevris V (eds) Computational methods in earthquake engineering, computational methods in applied sciences. Springer, Dordrecht

Applied Technology Council (1978) ATC3: tentative provisions for the development of seismic regulations for buildings. Washington, DC
ASCE (2022) ASCE/SEI 7–10: minimum design loads for buildings and other structures. Reston, VA
Bianchi S, Ciurlanti J, Perrone D et al (2021) Shake-table tests of innovative drift sensitive nonstructural elements in a low-damage structural system. Earthq Eng Struct Dyn 50(9):2398–2420
Calvi PM, Sullivan TJ (2014) Estimating floor spectra in multiple degree of freedom systems. Earthq Struct 7(1):17–38
Carr AJ (2017) Ruaumoko user's manual for the 2-dimensional version. Carr Research Limited, Christchurch
CEN (2004) Eurocode 8: design of structures for earthquake resistance. Part 1: general rules, seismic actions and rules for buildings. Belgium, Brussels
CEN (2018) Eurocode 2: design of concrete structures - part 4: design of fastenings for use in concrete. Belgium, Brussels
Ciurlanti J, Bianchi S, Pürgstaller A, Quintana Gallo P, Bergmeister K, Pampanin S (2022) Shake table tests of concrete anchors including innovative and alternative anchorage detailing. Bull Earthq Eng 20:3971–3993
Cowan H et al (2011) The M8.8 Chile earthquake, 27 February 2010. Bull NZ Soc Earthq Eng 44(3):123–166
Douglas H (2010) Inductive risk and values in science. Philos Sci 67(4):559–579
Eligehausen R, Mallée R, Silva JF (2006) Anchorage in concrete construction. Ernst and Sohn Publisher, Berlin
FEMA E-74 (2012) Reducing the risks of nonstructural earthquake damage – a practical guide. Federal Emergency Management Agency, Washington
Hoehler M (2006) Behavior and testing of fastenings to concrete for use in seismic applications. In: PhD thesis, Institut für Werkstoffe im Bauwesen, Universität Stuttgart, Germany
INN (Instituto Nacional de Normalización) (1996) NCh433Of.96: seismic design of buildings. Santiago, Chile (**in Spanish**)
INN (Instituto Nacional de Normalización) (2012) NCh433Of.96mod2012: seismic design of buildings. Santiago, Chile (**in Spanish**)
Lorenz E (1963) Deterministic nonperiodic flow. J Atmos Sci 20:130–141
Mahrenholtz P (2013) Experimental performance and recommendations for qualification of post-installed anchors for seismic applications. In: PhD thesis, Institut für Werkstoffe im Bauwesen, Universität Stuttgart, Germany
Ministero delle Infrastrutture dei Trasporti, MIT (2018). Aggiornamento delle Norme Tecniche per le Costruzioni, Supplemento ordinario n°8 alle G.U. n° 42 del 20/02/2018. Rome, Italy (In Italian)
Pampanin S (2012) Reality-check and renewed challenges in earthquake engineering: Implementing low-damage structural systems – from theory to practice. Bull NZ Soc Earthq Eng 45(4):137–160
Pürgstaller A, Quintana Gallo P, Pampanin S, Bergmeister K (2020) Seismic demands on non-structural components anchored to concrete accounting for structure-fastener-nonstructural interaction (SFNI). Earthq Eng Struct Dyn 49(6):589–606
Pürgstaller A. (2017) Seismic performance of post-installed fasteners in concrete with supplemental damping device at structure-fastener-nonstructural-(SFN)-level. In: PhD thesis, University of Natural Resources and Life Sciences, Vienna, Austria
Quintana Gallo P, Meneses R (2021) On stability of SDOF system with asymmetric hysteresis subjected to seismic excitations. Int J Struct Stab Dyn 21(5):2171002
Quintana Gallo P, Moghaddasi M, Pampanin S, Bergmeister K (2018) Shake table tests of post-installed anchors with supplemental damping. ACI Struct J 115(1):595–606
Quintana Gallo P, Moghaddasi M, Pampanin S, Carr AJ (2019) Hysteresis model for concrete anchors subjected to shear loading. ACI Struct J 116(1):5–16
Quintana Gallo P, Bonelli P, Pampanin S, Carr AJ (2020) Seismic design of RC walls in Chile: damage observations and identified deficiencies after the 2010 Maule Earthquake. Report 2020-01. University of Canterbury, Christchurch
Quintana Gallo P, Carradine DM (2021) Philosophical reflexions following the Lyttleton 2011 New Zealand earthquake: ten years after. In: Proc 2021 NZ Soc Earthq Eng Conference, Christchurch
Quintana Gallo P (2008) Evaluación analítica del daño en un edificio de Hormigón Armado. In: Magister thesis, Universidad Técnica Federico Santa María, Valparaiso, Chile
Rojas D (2020) Evaluación de la respuesta sísmica de elementos no-estructurales (NSC) anclados a edificios de hormigón armado incluyendo la histéresis de la connexion. Trabajo de Título. Universidad de Valparaíso, Valparaíso (**In Spanish**)
Rudner R (1953) The scientist qua scientist makes value judgements. Philos Sci 20(1):1–6

Saiidi M, Sozen MA (1979) Simple and complex models for nonlinear seismic response of reinforced concrete structures. Report UILU-ENG-79–2031. University of Illinois Urbana, Champaign
Standards New Zealand (SNZ) (2004) NZS1170.5:2004: structural design actions: part 5, earthquake actions. Wellington, New Zealand
Standards New Zealand (SNZ) (2006) NZS3101.1:2006: concrete structures standard: Part 1, the design of concrete structures. Wellington, New Zealand
Sullivan TJ, Calvi PM, Nascimbene R (2013) Towards improved floor spectra estimates for seismic design. Earthq Struct 4(1):109–132
Taghavi S, Miranda E (2003) Response assessment of non-structural building elements. PEER report 2003/05. Pacific Earthquake Engineering Research Center, Berkeley
Villaverde R (1997) Seismic design of secondary structures: state of the art. J Struct Eng 123(8):1011–1019
Whittaker A, Soong TT (2003). An overview of nonstructural research at three U.S. Earthquake Engineering Research Centers. In: ATC-29–2 Seminar on the Seismic Design, Performance and Retrofit of Nonstructural Components in Critical Facilities, Irvine, CA

Authors and Affiliations

D. Rojas[1] · P. Quintana Gallo[2] · A. Pürgstaller[3] · S. Bianchi[4] · J. Ciurlanti[5] · S. Pampanin[6] · K. Bergmeister[7]

1 School of Civil Engineering, University of Valparaiso, Valparaiso, Chile

2 Department of Steel and Timber Structures, Czech Technical University in Prague, Prague, Czech Republic

3 Bergmeister Ingenieure GmbH, Munich, Germany

4 Department of Structural Design and Mechanics, Delft University of Technology, Delft, The Netherlands

5 ARUP, Amsterdam, The Netherlands

6 Department of Structural and Geotechnical Engineering, Sapienza University, Rome, Italy

7 Institute of Structural Engineering, University of Natural Resources and Life Sciences, Vienna, Austria